# STAR-RIS Aided Covert Communication in UAV Air-Ground Networks

Qunshu Wang, Shaoyong Guo, *Member, IEEE*, Celimuge Wu, *Senior Member, IEEE*, Chengwen Xing, *Member, IEEE*, Nan Zhao, *Senior Member, IEEE*, Dusit Niyato, *Fellow, IEEE*, and George K. Karagiannidis, *Fellow, IEEE*.

***Abstract*—The combination of a simultaneously transmitting and reflecting reconfigurable intelligent surface (STAR-RIS) and an unmanned aerial vehicle (UAV) can further improve channel quality and extend coverage. However, the high-quality air-to-ground link is more vulnerable to eavesdropping by adversaries. In this paper, we investigate STAR-RIS-assisted covert communication in UAV non-orthogonal multiple access (NOMA) networks with a warden Willie, where Alice intends to transmit the covert signal to a near user Bob under the cover of a far user Carol via STAR-RIS. We aim to maximize the covert transmission rate by jointly optimizing the active and passive beamforming as well as the UAV location. The error detection probability and optimal detection threshold for Willie are first derived to obtain an analytic solution for the minimum detection error probability. Then, an alternating optimization algorithm is proposed to maximize the covert transmission rate under the condition of guaranteeing the communication of Carol and satisfying the covertness constraint of Bob. Specifically, the nonconvex problem is decomposed into three sub-problems by block coordinate descent, which are then solved using semidefinite relaxation and successive convex approximation. Finally, simulation results are presented to demonstrate the effectiveness of the proposed covert communication scheme for STAR-RIS assisted UAV air-ground networks.**

Manuscript received February 08, 2024; revised May 29, 2024; accepted August 05, 2024. The work of Nan Zhao is supported in part by the National Natural Science Foundation of China (NSFC) under Grant U23A20271. The work of Chengwen Xing is supported in part by the National Natural Science Foundation of China (NSFC) under Grant 62325103. The work of Celimuge Wu is supported in part by JST ASPIRE Grant Number JPMJAP2325, and in part by ROIS NII Open Collaborative Research under Grant 24S0601. The work of Dusit Niyato is supported by the National Research Foundation, Singapore, and Infocomm Media Development Authority under its Future Communications Research & Development Programme, Defence Science Organisation (DSO) National Laboratories under the AI Singapore Programme (AISG Award No: AISG2-RP-2020-019 and FCP-ASTAR-TG-2022-003), Singapore Ministry of Education (MOE) Tier 1 (RG87/22), and the NTU Centre for Computational Technologies in Finance (NTU-CCTF). *(Corresponding author: Nan Zhao.)*

Qunshu Wang and Nan Zhao are with the School of Information and Communication Engineering, Dalian University of Technology, Dalian 116024, China (e-mail: wangqunshu@mail.dlut.edu.cn; zhaonan@dlut.edu.cn).

Shaoyong Guo is with the State Key Laboratory of Networking and Switching Technology, Beijing University of Posts and Telecommunications, Beijing 100876, China (e-mail: syguo@bupt.edu.cn).

Celimuge Wu is with the Department of Computer and Network Engineering, The University of Electro-Communications, Chofu, Tokyo 182-8585, Japan (e-mail: celimuge@uec.ac.jp).

Chengwen Xing is with the School of Information and Electronics, Beijing Institute of Technology, Beijing 100081, China (e-mail: xingchengwen@gmail.com).

Dusit Niyato is with the College of Computing and Data Science, Nanyang Technological University, Singapore 639798 (e-mail: dniyato@ntu.edu.sg).

George K. Karagiannidis is with Department of Electrical and Computer Engineering, Aristotle University of Thessaloniki, Greece and also with Artificial Intelligence & Cyber Systems Research Center, Lebanese American University (LAU), Lebanon (e-mail: geokarag@auth.gr).

***Index Terms*—Air-ground networks, covert communication, non-orthogonal multiple access, simultaneously transmitting and reflecting reconfigurable intelligent surface, unmanned aerial vehicle.**

## I. Introduction

The sixth generation (6G) mobile communication aims at building a space-air-ground integrated network (SAGIN) to further realize the global coverage [1]. As a significant part of the integrated network, unmanned aerial vehicle (UAV) aided air-ground networks have been widely utilized in the civilian, commercial, and even military fields, e.g., fire rescue, cargo transportation, remote control and aerial reconnaissance [2] [3]. Compared with the traditional terrestrial base stations (BSs), UAVs as airborne BSs can not only be used in remote areas or dense environments to improve the channel quality, but also provide short-term high-speed connections during disasters [4]. However, with the improvement of communication quality, the security of UAV air-ground networks urgently needs to be improved. Ding *et al.* in [5] maximized the secure computational efficiency of UAV-based mobile edge computing (MEC). The security performance of dual UAV networks was investigated by Lei *et al.* in [6]. Considering multiple eavesdroppers, Li *et al.* in [7] investigated the average minimum secrecy rate maximization of multi-UAV networks.

All the above research works are carried out from the perspective of physical layer security (PLS), and only focus on hiding the communication information. However, in many specific scenarios, it is necessary to hide the communication behavior [8]. The emerging covert communication can well address this issue and provide a higher level of security for wireless communication. Given this advantage, covert communication in UAV-assisted air-ground networks has attracted much attention from both academia and industry [9]–[13]. In [9], Zhou *et al.* applied a UAV to extend the applications of covert communication from static to dynamic. To expand the scope of covert communication, Jiao *et al.* in [10] presented a UAV relay assisted covert transmission scheme and maximized the effective covert throughput. The full-duplex UAV was utilized by Li *et al.* in [11] to further enhance the covertness of UAV-assisted relaying. Considering the uncertainty of Willie's position, Yang *et al.* in [12] maximized the average covert rate of a dual-UAV covert communication system. In [13], Hu *et al.* jointly optimized the transmit power and the UAV trajectory to maximize the covert throughput.

Despite the outstanding advantages of UAV-based covert networks, the air-ground line-of-sight (LoS) links provided by UAVs can be easily affected, especially in the complex propagation environment [14]. Benefiting from the gradual maturation of metasurface and its related fabrication technology, the emergence and development of reconfigurable intelligent surface (RIS) makes up for this deficiency [15], [16]. Compared with the conventional active radio frequency source, the superiority of RIS is that it is more economical and environmentally friendly, as it only passively reflects the incident signals [17], [18]. In addition, RIS is easy to deploy and can be seamlessly embedded in various locations, such as billboards, skyscrapers, and windows [19]. In order to construct a full-space intelligent propagation environment, the simultaneous transmitting and reflecting RIS (STAR-RIS) is investigated by Liu *et al.* in [20]. Compared with the conventional RIS, STAR-RIS can both reflect and transmit signals, which can not only extend the coverage, but also have a wider range of applications [21], [22].

Considering the above advantages, introducing STAR-RIS into UAV networks can not only improve the transmission quality, but also expand the coverage, which is more conducive to the deep integration between airborne platforms and terrestrial networks [23]. In addition, the integration between STAR-RIS and UAV is likely to be more cost-effective than terrestrial BSs, which further saves the treasurable resource for SAGIN. According to the installation modes of STAR-RIS, the combination of UAV and STAR-RIS mainly includes two paradigms: STAR-RIS assisted UAV communication and UAV-mounted STAR-RIS communication. In STAR-RIS assisted UAV communication systems [24], [25], the STAR-RIS installed on the surface of buildings can add a cascaded channel between UAV and users to further improve the channel quality. Su *et al.* in [24] verified that the sum rate of users in UAV networks with STAR-RIS is superior to those with the conventional RIS. In [25], Zhu *et al.* proposed an alternating optimization (AO) algorithm to maximize the sum rate of UAV-supported STAR-RIS networks. In UAV-mounted STAR-RIS communication systems [26], [27], the STAR-RIS installed on UAVs can improve its flexibility and bring new degrees of freedom (DoF). In [26], Xiao *et al.* mounted the STAR-RIS on a UAV to improve the energy efficiency (EE) of MEC networks. The average achievable sum rate of users for UAV-mounted STAR-RIS-assisted terahertz systems was maximized by Wang *et al.* in [27].

Although the combination of UAV and STAR-RIS can further improve the performance, it can also increase the risk of eavesdropping by adversaries. In [28], Wang *et al.* maximized the secrecy EE (SEE) of an intelligent omni-surface (IOS) assisted UAV system. The average secrecy rate maximization of an IOS-assisted UAV system was investigated by Benaya *et al.* in [29]. Guo *et al.* in [30] demonstrated that UAV-mounted STAR-RIS systems can achieve higher SEE compared to the fixed STAR-RIS. However, all of the above research works are analyzed from the perspective of PLS. To the best of our knowledge, the research on UAV-assisted STAR-RIS covert communication is still vacant. In contrast to existing work on UAV-RIS covert communication, STAR-RIS can further improve the communication rate of an indoor user while counteracting the warden. Therefore, the UAV-assisted STAR-RIS covert communication framework is worth studying. In addition, non-orthogonal multiple access (NOMA) can be applied to further enhance the covertness, as it can use the distant user's signal as interference to hide the near user's signal [31].

Motivated by this, in this paper, we propose an STAR-RIS-assisted UAV air-ground covert communication scheme where a UAV serving as Alice sends the covert signal to an outdoor user Bob and the public signal to an indoor user Carol with STAR-RIS. Then, our goal is to maximize the covert transmission rate of Bob by jointly optimizing the transmit beamforming, the passive beamforming of STAR-RIS, and the UAV location. The comparison between our work and other similar works is illustrated in Table I and the main contributions of this thesis are summarized as follows.

- We present an STAR-RIS-assisted UAV-NOMA covert communication scheme with a guard Willie, where the signal of a public user in NOMA is used as a mask to hide a covert user to counter an interceptor. The UAV position and the phase shifts of STAR-RIS can be used to weaken the guard's detection of the covert signal.
- Considering the noise uncertainty of Willie, we analyze his detection performance. Specifically, the optimal detection threshold for Willie is derived and the analytic solution of minimum detection error probability (MDEP) is acquired. To facilitate the subsequent optimization, we reduce the covertness constraint to a manageable form. Then, we formulate a covert transmission rate maximization problem while satisfying the QoS of Carol and the covertness constraint of Bob.
- Using the block coordinate descent (BCD) method, the original non-convex problem can be decoupled into three subproblems, which can be resolved by the semidefinite relaxation (SDR) and successive convex approximation (SCA). In addition, an AO algorithm is presented to iteratively find the optimal solution. Finally, simulation results indicate that the proposed covert communication scheme can effectively enhance the covert transmission rate of STAR-RIS assisted UAV air-ground networks.

The remainder of the paper is organized as follows. In Section II, the STAR-RIS aided UAV-NOMA covert communication system and the channel model are presented. The optimal detection threshold for Willie is derived and the MDEP is acquired in Section III. In Section IV, a covert transmission rate maximization problem is formulated and solved by the AO algorithm. The effectiveness of the proposed scheme is shown via simulations in Section V. Finally, in Section VI, we conclude the paper.

*Notations:* Vectors and matrices are expressed by the bold lowercase and uppercase letters, respectively. $\Pr(\cdot)$ stands for the probability operation for solving the random variables. The conjugate and Hermitian transpose operators are denoted using $(\cdot)^*$ and $(\cdot)^H$. The absolute value of a complex scalar is indicated by $|\cdot|$ and the Euclidean norm of a vector is represented as $\|\cdot\|$. $\otimes$ is the Kronecker product. $\mathrm{diag}(\mathbf{a})$

TABLE I: Comparison between this work and other similar works.

| Reference | NOMA | Security | BS | Number of antennas | Algorithm | Metric |
|---|---|---|---|---|---|---|
| [24] | w/ | w/o | Aerial | Single antenna | AO based on SDR and SCA | Sum rate |
| [25] | w/o | w/o | Aerial | Single antenna | AO based on the penalty method and SCA | Achievable sum rate |
| [26] | w/o | w/o | Terrestrial | Single antenna | AO based on Dinkelbach and SCA | Energy efficiency |
| [27] | w/o | w/o | Terrestrial | Multiple antennas | 3D optimal position finding | Average achievable sum rate |
| [28] | w/ | PLS | Terrestrial | Single antenna | AO based on SROCR[1], SCA and B&B[2] | Secrecy energy efficiency |
| [29] | w/o | PLS | Terrestrial | Single antenna | SCA | Average secrecy rate |
| [30] | w/ | PLS | Terrestrial | Single antenna | DDQN[3] | Secrecy energy efficiency |
| Our work | w/ | Covertness | Aerial | Multiple antennas | AO based on SDR and SCA | Covert transmission rate |

[1]SROCR: sequential rank-one constraint relaxation, [2]B&B: branch-and-bound, [3]DDQN: double deep Q-network.

denotes a diagonal matrix whose diagonal elements originate from $\mathbf{a}$.

## II. System and Channel Models

In this section, we first present an STAR-RIS aided UAV-NOMA network with a warden to realize the covert air-ground transmission between Alice and Bob with the cover from Carol. Then, the system and channel models of the covert communication are described.

### A. System Model

Figure 1 illustrates an STAR-RIS-assisted UAV-NOMA network for covert communication, where a UAV (Alice) enables covert air-ground transmission to an outdoor user (Bob) and public transmission to an indoor user (Carol)[1], under surveillance by a warden (Willie). There is no direct link between Alice and Carol since Carol is located inside the building. Alice transmits a public signal to Carol as a cover to realize the covert communication between Alice and Bob. Consider that Alice is equipped with $N_a$ antennas and the other nodes are all equipped with a single antenna[2]. Adopting the three-dimension (3D) Cartesian coordinate, the coordinates of STAR-RIS, Alice, Bob, Carol and Willie are denoted as $\mathbf{q}_r = [x_r, y_r, H_r]^T$, $\mathbf{q}_a = [x_a, y_a, H_a]^T$, $\mathbf{q}_b = [x_b, y_b, 0]^T$, $\mathbf{q}_c = [x_c, y_c, H_c]^T$ and $\mathbf{q}_w = [x_w, y_w, 0]^T$, respectively.

The STAR-RIS is composed of a uniform planar array (UPA) with $M = M_x \times M_z$ reflecting elements, where $M$ is the total number of transmission and reflection elements, and $M_x$ and $M_z$ are the number of elements along $x$-axis and $z$-axis, respectively. The transmission- and reflection-coefficient matrices of STAR-RIS are defined as $\mathbf{\Phi}_t \in \mathbb{C}^{M\times M}$ and $\mathbf{\Phi}_r \in \mathbb{C}^{M\times M}$, where $\mathbf{\Phi}_t = \sqrt{\beta_t}\text{diag}\left(e^{j\theta_1^t}, e^{j\theta_2^t}, \cdots, e^{j\theta_M^t}\right)$ and $\mathbf{\Phi}_r = \sqrt{\beta_r}\text{diag}\left(e^{j\theta_1^r}, e^{j\theta_2^r}, \cdots, e^{j\theta_M^r}\right)$. $\beta_t$ and $\beta_r$ denote the transmitted and reflected amplitude coefficients of STAR-RIS. $\theta_m^t$ and $\theta_m^r \in [0, 2\pi)$, $\forall m \in \mathcal{M}$, $\mathcal{M} = \{1, \cdots, M\}$, represent the transmitted and reflected phase shifts of STAR-RIS[3].

[1]The proposed scenario is just a representative for more general cases, and the considered system model can be easily extended for other scenarios. Depending on the location of STAR-RIS, the proposed system has different application scenarios for SAGIN.

[2]The model can be well extended to the case of applying multiple antennas at other nodes, which will be investigated in our future work.

[3]Without loss of generality, the independent reflected and transmitted phase-shift model, as an upper bound of the coupled phase-shift model, is taken into account [22]. The more practical coupled model in our future study will be considered.

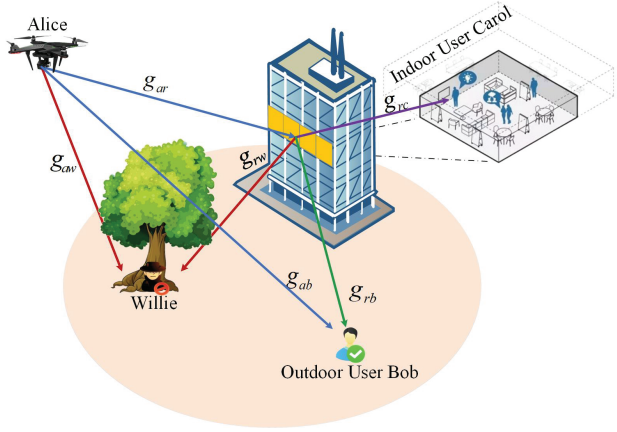


Fig. 1: Covert communication in the STAR-RIS aided UAV-NOMA network with a warden.

Owing to the energy splitting (ES) protocol, $\beta_r, \beta_t \in [0, 1]$ and $\beta_r + \beta_t = 1$ should be satisfied.

### B. Channel Model

Since both the UAV and STAR-RIS are located at high positions, the channel between them can be regarded as LoS links. Consequently, the channel gain $\mathbf{g}_{ar}$ can be modeled as

$$\mathbf{g}_{ar} = \sqrt{\rho_0 d_{ar}^{-2}}\mathbf{a}_M^T\mathbf{a}_{N_a} \in \mathbb{C}^{M\times N_a}, \tag{1}$$

where $\rho_0$ represents the path-loss at the reference distance $d_0 = 1$ m, and $d_{ar} = \|\mathbf{q}_a - \mathbf{q}_r\|$ is the distance between Alice and STAR-RIS. When the signal arrives at the STAR-RIS, the array response $\mathbf{a}_M$ can be defined as

$$\mathbf{a}_M = \left[1, \cdots, e^{-j\frac{2\pi}{\lambda}\tilde{d}_x(M_x-1)\sin\varphi_{ar}\cos\phi_{ar}}\right] \otimes \left[1, \cdots, e^{-j\frac{2\pi}{\lambda}\tilde{d}_z(M_z-1)\cos\varphi_{ar}}\right], \tag{2}$$

where $\lambda$ denotes the carrier wavelength, and $\tilde{d}_x$ and $\tilde{d}_z$ are the element spacing of STAR-RIS along $x$-axis and $z$-axis, respectively. $\varphi_{ar}$ and $\phi_{ar}$ are the azimuth angle of arrival (AoA) and the elevation AoA from Alice to STAR-RIS with

$$\sin\varphi_{ar}\cos\phi_{ar} = \frac{x_r - x_a}{d_{ar}}, \tag{3}$$

and

$$\cos\varphi_{ar} = \frac{H_r - H_a}{d_{ar}}. \tag{4}$$

Considering a uniform linear array (ULA) of antennas at Alice, the array response $\mathbf{a}_{N_a}$ can be represented as

$$\mathbf{a}_{N_a} = \left[1, e^{-j\frac{2\pi}{\lambda}\tilde{d}\cos\phi_a}, \cdots, e^{-j\frac{2\pi}{\lambda}\tilde{d}(N_a-1)\cos\phi_a}\right], \quad (5)$$

where $\tilde{d}$ denotes the antenna spacing and $\phi_a$ is the angle-of-departure (AoD) with $\cos\phi_a = (x_r - x_a)/d_{ar}$.

As a warden, Willie does not expect to be detected by the legitimate nodes as it tends to hide himself, such as behind a tree or a building. Therefore, the channels from the STAR-RIS and Alice to Willie can be modeled as the Rayleigh fading as

$$\mathbf{g}_{rw}^H = \sqrt{\rho_0 d_{rw}^{-\nu_1}}\mathbf{h}_{rw}^H \in \mathbb{C}^{1\times M}, \quad (6)$$

and

$$\mathbf{g}_{aw}^H = \sqrt{\rho_0 d_{aw}^{-\nu_1}}\mathbf{h}_{aw}^H \in \mathbb{C}^{1\times N_a}, \quad (7)$$

where $\nu_1$ is the path-loss exponent, and $d_{rw} = \|\mathbf{q}_r - \mathbf{q}_w\|$ and $d_{aw} = \|\mathbf{q}_a - \mathbf{q}_w\|$ are the distances from the STAR-RIS and Alice to Willie, respectively. $\mathbf{h}_{rw} \triangleq [h_{rw_1}, \cdots, h_{rw_M}]$ contains the channel gain for each element, which can be modeled as the independent and identically distributed complex Gaussian distribution, i.e., $\mathbf{h}_{rw} \sim \mathcal{CN}(0, \mathbf{I}_M)$. Similarly, $\mathbf{h}_{aw} \sim \mathcal{CN}(0, \mathbf{I}_{N_a})$.

Assume that the LoS links between Alice and Bob are obstructed by various obstacles such as skyscrapers and trees. Therefore, the Rayleigh fading is employed to model it, which can be expressed as

$$\mathbf{g}_{ab}^H = \sqrt{\rho_0 d_{ab}^{-\nu_1}}\mathbf{h}_{ab}^H \in \mathbb{C}^{1\times N_a}, \quad (8)$$

where $d_{ab} = \|\mathbf{q}_a - \mathbf{q}_b\|$ stands for the distance between Alice and Bob, and $\mathbf{h}_{ab}$ follows the complex Gaussian distribution with zero mean and unit variance.

Since the STAR-RIS can improve the channel conditions with its passive beamforming, we assume that the channel links from the STAR-RIS to Bob and Carol contain both LoS and NLoS components. Therefore, $\mathbf{g}_{ri}^H \in \mathbb{C}^{1\times M}, i \in \{b, c\}$ is modeled as Rician fading, which can be given by

$$\mathbf{g}_{ri}^H = \sqrt{\rho_0 d_{ri}^{-\nu_2}}\left(\sqrt{\frac{\mathcal{K}}{\mathcal{K}+1}}\bar{\mathbf{g}}_{ri}^{LoS} + \sqrt{\frac{1}{\mathcal{K}+1}}\tilde{\mathbf{g}}_{ri}^{NLoS}\right), \quad (9)$$

where $\nu_2$ is the path-loss exponent, $d_{ri} = \|\mathbf{q}_r - \mathbf{q}_i\|$ is the distance between the STAR-RIS and user $i$, and $\mathcal{K}$ denotes the Rician factor. The LoS component of $\mathbf{g}_{ri}$ can be expressed as

$$\begin{aligned}\bar{\mathbf{g}}_{ri}^{LoS} = &\left[1, \cdots, e^{-j\frac{2\pi}{\lambda}\tilde{d}_x(M_x-1)\sin\varphi_{ri}\cos\phi_{ri}}\right] \\ &\otimes \left[1, \cdots, e^{-j\frac{2\pi}{\lambda}\tilde{d}_z(M_z-1)\cos\varphi_{ri}}\right], \end{aligned} \quad (10)$$

where $\varphi_{ri}$ and $\phi_{ri}$ are the azimuth AoA and the elevation AoA from the STAR-RIS to user $i$, respectively,

$$\sin\varphi_{ri}\cos\phi_{ri} = \frac{x_i - x_r}{d_{ri}}, \quad (11)$$

and

$$\cos\varphi_{ri} = \frac{H_i - H_r}{d_{ri}}. \quad (12)$$

Furthermore, its NLoS component $\tilde{\mathbf{g}}_{ri}^{NLoS}$ can be modeled as the complex Gaussian distribution, i.e., $\tilde{\mathbf{g}}_{ri}^{NLoS} \sim \mathcal{CN}(0, \mathbf{I}_M)$.

### C. Received Signals at NOMA Users

For the $k$-th channel, $\forall k \in \{1, \cdots, K\}$, Alice sends the superimposed signal $\mathbf{w}_1 x_1[k] + \mathbf{w}_2 x_2[k]$ to the two NOMA users where $\mathbf{w}_1 \in \mathbb{C}^{N_a\times 1}$ and $\mathbf{w}_2 \in \mathbb{C}^{N_a\times 1}$ are the beamforming vectors at Alice, satisfied with $\|\mathbf{w}_1\|^2 + \|\mathbf{w}_2\|^2 \le P_a$. $P_a$ denotes the maximum transmit power at Alice. $x_1[k]$ and $x_2[k]$ represent the intended signals of Bob and Carol for the $k$-th channel respectively, which can be modeled by the Gaussian signal with zero mean and unit variance, and $K$ is the total number of channels. Then, the received signals at Bob and Carol can be given by

$$y_b[k] = \left(\mathbf{g}_{rb}^H \mathbf{\Phi}_\mathbf{r} \mathbf{g}_{ar} + \mathbf{g}_{ab}^H\right)(\mathbf{w}_1 x_1[k] + \mathbf{w}_2 x_2[k]) + z_b[k], \quad (13)$$

and

$$y_c[k] = \mathbf{g}_{rc}^H \mathbf{\Phi}_t \mathbf{g}_{ar}(\mathbf{w}_1 x_1[k] + \mathbf{w}_2 x_2[k]) + z_c[k], \quad (14)$$

where $z_b[k] \sim \mathcal{CN}(0, \sigma_b^2)$ and $z_c[k] \sim \mathcal{CN}(0, \sigma_c^2)$ denote the additive white Gaussian noise (AWGN) at Bob and Carol, respectively.

As a near user, Bob first decodes the desired signal $x_2$ of far user Carol, and then decodes its own signal $x_1$. Therefore, the received signal-to-interference-plus-noise ratio (SINR) at Bob to decode $x_2$ can be expressed as

$$\gamma_{b\to c} = \frac{\left|\left(\mathbf{g}_{rb}^H \mathbf{\Phi}_r \mathbf{g}_{ar} + \mathbf{g}_{ab}^H\right)\mathbf{w}_2\right|^2}{\left|\left(\mathbf{g}_{rb}^H \mathbf{\Phi}_r \mathbf{g}_{ar} + \mathbf{g}_{ab}^H\right)\mathbf{w}_1\right|^2 + \sigma_b^2}. \quad (15)$$

Utilizing the successive interference cancellation (SIC), the received SINR at Bob to decode $x_1$ can be denoted as

$$\gamma_b = \frac{\left|\left(\mathbf{g}_{rb}^H \mathbf{\Phi}_r \mathbf{g}_{ar} + \mathbf{g}_{ab}^H\right)\mathbf{w}_1\right|^2}{\sigma_b^2}. \quad (16)$$

For Carol, it just needs to decode its own signal. Consequently, the received SINR at Carol to decode $x_2$ can be given by

$$\gamma_c = \frac{\left|\mathbf{g}_{rc}^H \mathbf{\Phi}_t \mathbf{g}_{ar} \mathbf{w}_2\right|^2}{\left|\mathbf{g}_{rc}^H \mathbf{\Phi}_t \mathbf{g}_{ar} \mathbf{w}_1\right|^2 + \sigma_c^2}. \quad (17)$$

## III. Covert Analysis in STAR-RIS Aided UAV-NOMA Networks

In this section, we first conduct the binary hypothesis testing at Willie and analyze two error situations, i.e., the false alarm and miss detection. Then, we derive the optimal detection threshold to obtain an analytic solution for the MDEP. Finally, the covertness constraint is reduced to a manageable form to further optimize the covert transmission rate.

### A. Binary Hypothesis Testing at Willie

In the covert communication between Alice and Bob, Willie attempts to detect whether Alice is sending a covert signal to Bob via the Neyman-Pearson test. Consequently, Willie faces a binary hypothesis testing problem: 1) Alice is silent under circumstance of the null hypothesis $\mathcal{H}_0$, and 2) Alice is transmitting a covert signal to Bob under circumstance of the

alternative hypothesis $\mathcal{H}_1$. Then, the received signal at Willie for the $k$-th channel can be given by

$$y_w[k]=\begin{cases}\left(\mathbf{g}_{rw}^H\mathbf{\Phi}_r\mathbf{g}_{ar}+\mathbf{g}_{aw}^H\right)\mathbf{w}_2x_2\left[k\right]+z_w[k]\,, & \mathcal{H}_0,\\ \left(\mathbf{g}_{rw}^H\mathbf{\Phi}_r\mathbf{g}_{ar}+\mathbf{g}_{aw}^H\right)\left(\mathbf{w}_1x_1[k]+\mathbf{w}_2x_2[k]\right)+z_w[k], & \mathcal{H}_1,\end{cases} \tag{18}$$

where $\mathbf{g}_{rw}^H\mathbf{\Phi}_r\mathbf{g}_{ar}+\mathbf{g}_{aw}^H$ denotes the sum of the direct and cascaded channels from Alice to Willie, and $z_w\left[k\right]\sim\mathcal{CN}\left(0,\sigma_w^2\right)$ represents the AWGN at Willie. Since it is difficult to accurately obtain the AWGN power in practice, we consider the noise uncertainty at Willie, i.e., $\sigma_w^2$ is a random variable that obeys a uniform distribution in dB form [32]. Therefore, $\sigma_{w,\mathrm{dB}}^2\in\left[\tilde{\sigma}_{w,\mathrm{dB}}^2-\rho_{\mathrm{dB}},\tilde{\sigma}_{w,\mathrm{dB}}^2+\rho_{\mathrm{dB}}\right]$, where $\sigma_{w,\mathrm{dB}}^2=10\log_{10}\left(\sigma_w^2\right)$, $\tilde{\sigma}_{w,\mathrm{dB}}^2=10\log_{10}\left(\tilde{\sigma}_w^2\right)$, and $\rho_{\mathrm{dB}}=10\log_{10}\left(\rho\right)$. $\tilde{\sigma}_w^2$ denotes the nominal noise power, and $\rho$ represents a parameter used to measure the noise uncertainty with $\rho\geq1$. Then, the probability density function (PDF) of $\sigma_w^2$ can be expressed as

$$f_{\sigma_w^2}\left(x\right)=\begin{cases}\frac{1}{2\ln(\rho)x}, & \text{if } \frac{1}{\rho}\tilde{\sigma}_w^2\leq x\leq\rho\tilde{\sigma}_w^2,\\ 0, & \text{otherwise.}\end{cases} \tag{19}$$

In addition, we consider that Willie applies a radiometer to detect the received signal and carries out a threshold test for the average power $T_w$. Therefore, the adopted decision rule at Willie can be given by

$$T_w=\frac{1}{K}\sum_{k=1}^{K}\left\|y_w\left[k\right]\right\|^2\underset{\mathcal{D}_0}{\overset{\mathcal{D}_1}{\gtrless}}\tau, \tag{20}$$

where $\tau$ represents the detection threshold, and $\mathcal{D}_0$ and $\mathcal{D}_1$ are the detection results while supporting $\mathcal{H}_0$ and $\mathcal{H}_1$, respectively. It is important to select a reasonable $\tau$ for Willie's decision accuracy, which will be optimized later to minimize the detection error probability (DEP).

Similar to [33], we assume that the number of channels tends to infinity, i.e., $K\to\infty$, which means that an infinite number of samples can be observed by Willie. Since the number of transmitted symbols increases with the communication bandwidth, it is reasonable to assume that the number of channels approximately tends to be infinite by the choice of suitable bandwidth. Then, the average power $T_w$ at Willie can be rewritten as

$$T_w=\begin{cases}\left|\mathbf{G}_1\mathbf{w}_2\right|^2+\sigma_w^2, & \mathcal{H}_0,\\ \left|\mathbf{G}_1\mathbf{w}_1\right|^2+\left|\mathbf{G}_1\mathbf{w}_2\right|^2+\sigma_w^2, & \mathcal{H}_1,\end{cases} \tag{21}$$

where $\mathbf{G}_1=\mathbf{g}_{rw}^H\mathbf{\Phi}_r\mathbf{g}_{ar}+\mathbf{g}_{aw}^H$.

To better evaluate the detection performance, we denote two error situations, i.e., the false alarm and miss detection. If Willie mistakenly judges that Alice sends a covert signal to Bob while Alice keeps silent, the false alarm occurs. The probability of false alarm (PFA) can be represented as

$$P_{FA}\triangleq\Pr\left\{\mathcal{D}_1|\mathcal{H}_0\right\}=\Pr\left\{\left|\mathbf{G}_1\mathbf{w}_2\right|^2+\sigma_w^2\geq\tau\right\}. \tag{22}$$

If Alice sends a covert signal while Willie cannot detect it, the miss detection occurs. The probability of miss detection (PMD) can be expressed as

$$\begin{aligned}P_{MD}&\triangleq\Pr\left\{\mathcal{D}_0|\mathcal{H}_1\right\}\\&=\Pr\left\{\left|\mathbf{G}_1\mathbf{w}_1\right|^2+\left|\mathbf{G}_1\mathbf{w}_2\right|^2+\sigma_w^2\leq\tau\right\}.\end{aligned} \tag{23}$$

Consequently, the total DEP can be written as

$$\xi=P_{FA}+P_{MD}. \tag{24}$$

Willie attempts to acquire the MDEP $\xi^*$, while Alice has to ensure the MDEP being no less than a specific value, i.e., $\xi^*\geq1-\epsilon$, where $\epsilon\in[0,1]$ is a positive constant used to determine the covertness requirement.

### *B. Detection Performance at Willie*

Based on (22) and (23), the DEP can be given by

$$\xi=1-\Pr\left\{\tau-\phi_1\leq\sigma_w^2\leq\tau-\phi_2\right\}, \tag{25}$$

where $\phi_1=\left|\mathbf{G}_1\mathbf{w}_1\right|^2+\left|\mathbf{G}_1\mathbf{w}_2\right|^2$ and $\phi_2=\left|\mathbf{G}_1\mathbf{w}_2\right|^2$. To achieve the MDEP at Willie, the optimal detection threshold $\tau^*$ needs to be calculated. When $\tau<\phi_2+\frac{1}{\rho}\tilde{\sigma}_w^2$, $P_{FA}=1$ and $P_{MD}=0$, i.e., $\xi=1$, which signifies that Willie fails to detect the covert communication between Alice and Bob. Therefore, there is no MDEP in this region. When $\tau>\phi_2+\rho\tilde{\sigma}_w^2$, $P_{FA}=0$ and the value of $P_{MD}$ increases with $\tau$, which means $\tau^*\in\left[\phi_2+\frac{1}{\rho}\tilde{\sigma}_w^2,\phi_2+\rho\tilde{\sigma}_w^2\right]$. The optimal detection threshold is derived in Theorem 1.

**Theorem 1.** *The optimal detection threshold $\tau^*$ at Willie can be given by*

$$\tau^*=\min\left(\phi_1+\frac{1}{\rho}\tilde{\sigma}_w^2,\phi_2+\rho\tilde{\sigma}_w^2\right). \tag{26}$$

*Proof:* The detailed proof is presented in Appendix A. ■

Substituting (26) into (A.1) of Appendix A, the MDEP can be expressed as

$$\xi^*=\begin{cases}1-\frac{1}{2\ln(\rho)}\ln\left(1+\frac{\rho\phi}{\tilde{\sigma}_w^2}\right), & \phi\leq\tilde{\sigma}_w^2\left(\rho-\frac{1}{\rho}\right),\\ 0, & \text{otherwise,}\end{cases} \tag{27}$$

where $\phi=\phi_1-\phi_2=\left|\mathbf{G}_1\mathbf{w}_1\right|^2$. Since there is still a random variable $\phi$ in (27), we derive the analytic solution of MDEP, which is presented in Theorem 2.

**Theorem 2.** *The analytic solution of MDEP can be given by*

$$\xi^*=1-\frac{1}{2\ln\left(\rho\right)}\exp\left(\frac{1}{\rho\Delta}\right)E\left(\frac{\rho}{\Delta},\frac{1}{\rho\Delta}\right), \tag{28}$$

*where* $\Delta=\rho_0d_{aw}^{-v_1}\mathbf{w}_1^H\mathbf{w}_1+\frac{\rho_0d_{rw}^{-v_1}\mathbf{w}_1^H\mathbf{w}_1\mathrm{diag}(\mathbf{\Phi}_r)^H\mathrm{diag}(\mathbf{\Phi}_r)}{M}$.

*Proof:* The detailed proof is provided in Appendix B. ■

To ensure the covertness, $\xi^*\geq1-\epsilon$ has to be guaranteed. However, the analytic solution of MDEP is not conducive to the subsequent optimization. Therefore, we use (27) to get a manageable form, i.e., $\phi\leq\min\left(\frac{\left(\rho^{2\epsilon}-1\right)\tilde{\sigma}_w^2}{\rho},\frac{\left(\rho^2-1\right)\tilde{\sigma}_w^2}{\rho}\right)=\frac{\left(\rho^{2\epsilon}-1\right)\tilde{\sigma}_w^2}{\rho}$. Accordingly, the covertness constraint can be converted into $\left|\mathbf{G}_1\mathbf{w}_1\right|^2\leq\frac{\left(\rho^{2\epsilon}-1\right)\tilde{\sigma}_w^2}{\rho}$.

## IV. Problem Formulation and Algorithm Design

In this section, we first propose a covert transmission rate maximization problem under the circumstance of ensuring the QoS of Carol and meeting the covertness constraint. Then, owing to the complexity and non-convexity, we decouple the problem into three tractable sub-problems by the BCD method. Finally, the AO algorithm is employed to iteratively obtain the solution.

### A. Problem Formulation

By jointly optimizing the active beamforming $(\mathbf{w}_1, \mathbf{w}_2)$ at Alice, the passive beamforming $(\mathbf{\Phi}_r, \mathbf{\Phi}_t)$ of STAR-RIS, and the UAV location $\mathbf{q}_a$, the covert transmission rate maximization problem for the STAR-RIS aided UAV-NOMA network can be formulated as

$$\max_{\mathbf{w}_1,\mathbf{w}_2,\mathbf{\Phi}_r,\mathbf{\Phi}_t,\mathbf{q}_a} \log_2\left(1+\frac{\left|\left(\mathbf{g}_{rb}^H\mathbf{\Phi}_r\mathbf{g}_{ar}+\mathbf{g}_{ab}^H\right)\mathbf{w}_1\right|^2}{\sigma_b^2}\right) \tag{29a}$$

$$s.t. \quad \gamma_c \geq \gamma_{thc}, \tag{29b}$$

$$\gamma_{b\to c} \geq \gamma_{thc}, \tag{29c}$$

$$\|\mathbf{w}_1\|^2+\|\mathbf{w}_2\|^2 \leq P_a, \tag{29d}$$

$$|\mathbf{G}_1\mathbf{w}_1|^2 \leq \frac{\left(\rho^{2\epsilon}-1\right)\tilde{\sigma}_w^2}{\rho}, \tag{29e}$$

$$\beta_r+\beta_t=1, \beta_r, \beta_t \in [0,1], \tag{29f}$$

$$\theta_m^r, \theta_m^t \in [0,2\pi), \forall m \in \mathcal{M}, \tag{29g}$$

where $\gamma_{thc}=2^{R_{thc}}-1$ denotes the SINR threshold of Carol, and $R_{thc}$ represents the target rate of Carol. The constraint (29b) guarantees the QoS of Carol and the constraint (29c) ensures the success of SIC. The constraint (29d) is to ensure that the transmit power at Alice fails to exceed the maximum restriction. The constraint (29e) ensures the covertness performance between Alice and Bob. The constraint (29f) about the amplitudes of STAR-RIS is to meet the law of energy conservation and the constraint (29g) confines the phase shifts of STAR-RIS. It is difficult to obtain a globally optimal solution to (29) due to the tightly coupled optimization variables in the objective function and constraints. Therefore, we decouple it into three sub-problems as follows.

### B. Active Beamforming Optimization

For given $\mathbf{\Phi}_r$, $\mathbf{\Phi}_t$ and $\mathbf{q}_a$, the active beamforming optimization problem can be rewritten as

$$\max_{\mathbf{w}_1,\mathbf{w}_2} \log_2\left(1+\frac{\left|\left(\mathbf{g}_{rb}^H\mathbf{\Phi}_r\mathbf{g}_{ar}+\mathbf{g}_{ab}^H\right)\mathbf{w}_1\right|^2}{\sigma_b^2}\right) \tag{30a}$$

$$s.t. \quad \|\mathbf{w}_1\|^2+\|\mathbf{w}_2\|^2 \leq P_a, \tag{30b}$$

$$\frac{\left|\mathbf{g}_{rc}^H\mathbf{\Phi}_t\mathbf{g}_{ar}\mathbf{w}_2\right|^2}{\left|\mathbf{g}_{rc}^H\mathbf{\Phi}_t\mathbf{g}_{ar}\mathbf{w}_1\right|^2+\sigma_c^2} \geq \gamma_{thc}, \tag{30c}$$

$$\frac{\left|\left(\mathbf{g}_{rb}^H\mathbf{\Phi}_r\mathbf{g}_{ar}+\mathbf{g}_{ab}^H\right)\mathbf{w}_2\right|^2}{\left|\left(\mathbf{g}_{rb}^H\mathbf{\Phi}_r\mathbf{g}_{ar}+\mathbf{g}_{ab}^H\right)\mathbf{w}_1\right|^2+\sigma_b^2} \geq \gamma_{thc}, \tag{30d}$$

$$\left|\left(\mathbf{g}_{rw}^H\mathbf{\Phi}_r\mathbf{g}_{ar}+\mathbf{g}_{aw}^H\right)\mathbf{w}_1\right|^2 \leq \frac{\left(\rho^{2\epsilon}-1\right)\tilde{\sigma}_w^2}{\rho}. \tag{30e}$$

Although (30) has become a more concise form, its objective function and constraints are still non-convex. To transform the non-convex problem into a convex form, we first define $\mathbf{G}_2 = \mathbf{g}_{rb}^H\mathbf{\Phi}_r\mathbf{g}_{ar}+\mathbf{g}_{ab}^H$ and $\mathbf{G}_3=\mathbf{g}_{rc}^H\mathbf{\Phi}_t\mathbf{g}_{ar}$. Then, we have

$$|\mathbf{G}_2\mathbf{w}_1|^2=\mathbf{G}_2\mathbf{w}_1\mathbf{w}_1^H\mathbf{G}_2^H=\mathrm{Tr}\left(\mathbf{G}_2\mathbf{w}_1\mathbf{w}_1^H\mathbf{G}_2^H\right)=\mathrm{Tr}\left(\bar{\mathbf{G}}_2\mathbf{W}_1\right), \tag{31}$$

where $\bar{\mathbf{G}}_2 = \mathbf{G}_2^H\mathbf{G}_2$, and $\mathbf{W}_1 = \mathbf{w}_1\mathbf{w}_1^H$. Likewise, $|\mathbf{G}_2\mathbf{w}_2|^2 = \mathrm{Tr}\left(\bar{\mathbf{G}}_2\mathbf{W}_2\right)$, $|\mathbf{G}_3\mathbf{w}_1|^2 = \mathrm{Tr}\left(\bar{\mathbf{G}}_3\mathbf{W}_1\right)$, $|\mathbf{G}_3\mathbf{w}_2|^2 = \mathrm{Tr}\left(\bar{\mathbf{G}}_3\mathbf{W}_2\right)$ and $|\mathbf{G}_1\mathbf{w}_1|^2 = \mathrm{Tr}\left(\bar{\mathbf{G}}_1\mathbf{W}_1\right)$ hold when $\mathbf{W}_2=\mathbf{w}_2\mathbf{w}_2^H$, $\bar{\mathbf{G}}_1=\mathbf{G}_1^H\mathbf{G}_1$ and $\bar{\mathbf{G}}_3=\mathbf{G}_3^H\mathbf{G}_3$.

The problem (30) can be reformulated as

$$\max_{\mathbf{W}_1\succeq 0,\mathbf{W}_2\succeq 0} \log_2\left(1+\frac{\mathrm{Tr}\left(\bar{\mathbf{G}}_2\mathbf{W}_1\right)}{\sigma_b^2}\right) \tag{32a}$$

$$s.t. \quad \mathrm{Tr}\left(\mathbf{W}_1+\mathbf{W}_2\right) \leq P_a, \tag{32b}$$

$$\mathrm{Tr}\left(\bar{\mathbf{G}}_3\mathbf{W}_2\right) \geq \gamma_{thc}\left(\mathrm{Tr}\left(\bar{\mathbf{G}}_3\mathbf{W}_1\right)+\sigma_c^2\right), \tag{32c}$$

$$\mathrm{Tr}\left(\bar{\mathbf{G}}_2\mathbf{W}_2\right) \geq \gamma_{thc}\left(\mathrm{Tr}\left(\bar{\mathbf{G}}_2\mathbf{W}_1\right)+\sigma_b^2\right), \tag{32d}$$

$$\mathrm{Tr}\left(\bar{\mathbf{G}}_1\mathbf{W}_1\right) \leq \frac{\left(\rho^{2\epsilon}-1\right)\tilde{\sigma}_w^2}{\rho}, \tag{32e}$$

$$\mathrm{Rank}\left(\mathbf{W}_1\right)=\mathrm{Rank}\left(\mathbf{W}_2\right)=1. \tag{32f}$$

To observe the concavity and convexity of the objective function, we derive the second derivative of (32a) with respect to $\mathbf{W}_1$ as $\frac{-\left\|\bar{\mathbf{G}}_2^T\right\|^2}{\ln 2\left(\sigma^2+\mathrm{Tr}\left(\bar{\mathbf{G}}_2\mathbf{W}_1\right)\right)^2}$, which is less than zero, implying that (32a) is a concave function. However, the optimization problem is still non-convex due to the rank-one constraint of (32f). We remove the rank-one constraint by the SDR to acquire a tractable convex problem, and then resolve it via CVX. In Theorem 2, we verify that the ranks of optimal solutions $\mathbf{W}_1^*$ and $\mathbf{W}_2^*$ are 1, which indicates the tightness of SDR.

**Theorem 3.** *The optimal solutions $\mathbf{W}_1^*$ and $\mathbf{W}_2^*$, obtained by the SDR algorithm, satisfy* $\mathrm{Rank}\left(\mathbf{W}_1^*\right)=\mathrm{Rank}\left(\mathbf{W}_2^*\right)=1$ .

*Proof:* The detailed proof is provided in Appendix C. ■

### C. Passive Beamforming Optimization

For given $\mathbf{w}_1$, $\mathbf{w}_2$ and $\mathbf{q}_a$, the passive beamforming optimization can be given by

$$\max_{\mathbf{\Phi}_r,\mathbf{\Phi}_t} \log_2\left(1+\frac{\left|\left(\mathbf{g}_{rb}^H\mathbf{\Phi}_r\mathbf{g}_{ar}+\mathbf{g}_{ab}^H\right)\mathbf{w}_1\right|^2}{\sigma_b^2}\right) \tag{33a}$$

$$s.t. \quad \beta_r+\beta_t=1, \beta_r, \beta_t \in [0,1], \tag{33b}$$

$$\theta_m^r, \theta_m^t \in [0,2\pi), \forall m \in \mathcal{M}, \tag{33c}$$

$$(29b), (29c), (29e). \tag{33d}$$

For ease of expression, we make a series of transformations as follows:

$$\left|\mathbf{g}_{rc}^H\mathbf{\Phi}_t\mathbf{g}_{ar}\mathbf{w}_1\right|^2=\left|\mathbf{u}_t^H\mathbf{q}_3\right|^2=\mathrm{Tr}\left(\bar{\mathbf{q}}_3\bar{\mathbf{U}}_t\right), \tag{34}$$

$$\left|\mathbf{g}_{rc}^H\mathbf{\Phi}_t\mathbf{g}_{ar}\mathbf{w}_2\right|^2=\left|\mathbf{u}_t^H\mathbf{q}_4\right|^2=\mathrm{Tr}\left(\bar{\mathbf{q}}_4\bar{\mathbf{U}}_t\right), \tag{35}$$

where $\mathbf{u}_t=\left[\sqrt{\beta_t}e^{j\theta_1^t}, \sqrt{\beta_t}e^{j\theta_2^t}, \cdots, \sqrt{\beta_t}e^{j\theta_M^t}\right]^H$, $\bar{\mathbf{U}}_t=\mathbf{u}_t\mathbf{u}_t^H$, $\mathbf{q}_3=\mathrm{diag}\left(\mathbf{g}_{rc}^H\right)\mathbf{g}_{ar}\mathbf{w}_1$, $\mathbf{q}_4=\mathrm{diag}\left(\mathbf{g}_{rc}^H\right)\mathbf{g}_{ar}\mathbf{w}_2$, $\bar{\mathbf{q}}_3=\mathbf{q}_3\mathbf{q}_3^H$, and $\bar{\mathbf{q}}_4=\mathbf{q}_4\mathbf{q}_4^H$. In addition, let $\mathbf{p}_1=\mathbf{g}_{ab}^H\mathbf{w}_1$, $\mathbf{q}_1=\mathrm{diag}\left(\mathbf{g}_{rb}^H\right)\mathbf{g}_{ar}\mathbf{w}_1$,

and $\mathbf{u}_r = \left[\sqrt{\beta_r}e^{j\theta_1^r}, \sqrt{\beta_r}e^{j\theta_2^r}, \cdots, \sqrt{\beta_r}e^{j\theta_M^r}\right]^H$. Then, we have $\left|\left(\mathbf{g}_{rb}^H\mathbf{\Phi}_r\mathbf{g}_{ar}+\mathbf{g}_{ab}^H\right)\mathbf{w}_1\right|^2 = \left|\mathbf{u}_r^H\mathbf{q}_1+\mathbf{p}_1\right|^2$. We introduce two auxiliary variables as

$$\mathbf{R}_1 = \begin{bmatrix} \mathbf{q}_1\mathbf{q}_1^H & \mathbf{q}_1\mathbf{p}_1^H \\ \mathbf{p}_1\mathbf{q}_1^H & 0 \end{bmatrix}, \bar{\mathbf{u}}_r = \begin{bmatrix} \mathbf{u}_r \\ 1 \end{bmatrix}. \tag{36}$$

Thus, we have $\left|\mathbf{u}_r^H\mathbf{q}_1+\mathbf{p}_1\right|^2 = \mathrm{Tr}\left(\mathbf{R}_1\bar{\mathbf{U}}_r\right)+|\mathbf{p}_1|^2$, where $\bar{\mathbf{U}}_r = \bar{\mathbf{u}}_r\bar{\mathbf{u}}_r^H$.

Similarly, let $\mathbf{p}_2 = \mathbf{g}_{ab}^H\mathbf{w}_2$, $\mathbf{q}_2 = \mathrm{diag}\left(\mathbf{g}_{rb}^H\right)\mathbf{g}_{ar}\mathbf{w}_2$, $\mathbf{p}_3 = \mathbf{g}_{aw}^H\mathbf{w}_1$ and $\mathbf{q}_5 = \mathrm{diag}\left(\mathbf{g}_{rw}^H\right)\mathbf{g}_{ar}\mathbf{w}_1$. Then, we have $\left|\left(\mathbf{g}_{rb}^H\mathbf{\Phi}_r\mathbf{g}_{ar}+\mathbf{g}_{ab}^H\right)\mathbf{w}_2\right|^2 = \left|\mathbf{u}_r^H\mathbf{q}_2+\mathbf{p}_2\right|^2$ and $\left|\left(\mathbf{g}_{rw}^H\mathbf{\Phi}_r\mathbf{g}_{ar}+\mathbf{g}_{aw}^H\right)\mathbf{w}_1\right|^2 = \left|\mathbf{u}_r^H\mathbf{q}_5+\mathbf{p}_3\right|^2$. We also introduce another two auxiliary variables as

$$\mathbf{R}_2 = \begin{bmatrix} \mathbf{q}_2\mathbf{q}_2^H & \mathbf{q}_2\mathbf{p}_2^H \\ \mathbf{p}_2\mathbf{q}_2^H & 0 \end{bmatrix}, \mathbf{R}_3 = \begin{bmatrix} \mathbf{q}_5\mathbf{q}_5^H & \mathbf{q}_5\mathbf{p}_3^H \\ \mathbf{p}_3\mathbf{q}_5^H & 0 \end{bmatrix}. \tag{37}$$

We have $\left|\mathbf{u}_r^H\mathbf{q}_2+\mathbf{p}_2\right|^2 = \mathrm{Tr}\left(\mathbf{R}_2\bar{\mathbf{U}}_r\right)+|\mathbf{p}_2|^2$ and $\left|\mathbf{u}_r^H\mathbf{q}_5+\mathbf{p}_3\right|^2 = \mathrm{Tr}\left(\mathbf{R}_3\bar{\mathbf{U}}_r\right)+|\mathbf{p}_3|^2$.

Therefore, the problem (33) can be rewritten as

$$\max_{\bar{\mathbf{U}}_r,\bar{\mathbf{U}}_t} \ \log_2\left(1+\frac{\mathrm{Tr}\left(\mathbf{R}_1\bar{\mathbf{U}}_r\right)+|\mathbf{p}_1|^2}{\sigma_b^2}\right) \tag{38a}$$

$$s.t. \ \ \mathrm{Tr}\left(\bar{\mathbf{q}}_4\bar{\mathbf{U}}_t\right) \geq \gamma_{thc}\left(\mathrm{Tr}\left(\bar{\mathbf{q}}_3\bar{\mathbf{U}}_t\right)+\sigma_c^2\right), \tag{38b}$$

$$\mathrm{Tr}\left(\mathbf{R}_2\bar{\mathbf{U}}_r\right)+|\mathbf{p}_2|^2 \geq \gamma_{thc}\left(\mathrm{Tr}\left(\mathbf{R}_1\bar{\mathbf{U}}_r\right)+|\mathbf{p}_1|^2+\sigma_b^2\right), \tag{38c}$$

$$\mathrm{Tr}\left(\mathbf{R}_3\bar{\mathbf{U}}_r\right)+|\mathbf{p}_3|^2 \leq \frac{\left(\rho^{2\epsilon}-1\right)\tilde{\sigma}_w^2}{\rho}, \tag{38d}$$

$$\beta_r+\beta_t=1, \beta_r, \beta_t \in [0,1], \tag{38e}$$

$$\bar{\mathbf{U}}_r(m,m)=\beta_r, \bar{\mathbf{U}}_t(m,m)=\beta_t, \forall m \in \mathcal{M}, \tag{38f}$$

$$\bar{\mathbf{U}}_r(M+1,M+1)=1, \tag{38g}$$

$$\bar{\mathbf{U}}_r \succeq 0, \bar{\mathbf{U}}_t \succeq 0, \tag{38h}$$

$$\mathrm{Rank}\left(\bar{\mathbf{U}}_r\right)=\mathrm{Rank}\left(\bar{\mathbf{U}}_t\right)=1. \tag{38i}$$

Since the rank-one constraint is non-convex, we apply the SDR to relax it. As such, the optimization problem can be changed into an SDP, which can be solved via CVX. However, the optimal solution obtained by the SDR is difficult to satisfy the rank-one constraint. To solve this issue, we choose the Gaussian randomization to acquire a high-quality feasible solution. First, the eigenvalue decomposition of $\bar{\mathbf{U}}_r$ and $\bar{\mathbf{U}}_t$ can be represented as

$$\bar{\mathbf{U}}_r = \mathbf{V}_r\Sigma_r\mathbf{V}_r^H, \tag{39}$$

$$\bar{\mathbf{U}}_t = \mathbf{V}_t\Sigma_t\mathbf{V}_t^H, \tag{40}$$

where $\mathbf{V}_r \in \mathbb{C}^{(M+1)\times(M+1)}$ and $\mathbf{V}_t \in \mathbb{C}^{M\times M}$ denote unitary matrices, and $\Sigma_r \in \mathbb{C}^{(M+1)\times(M+1)}$ and $\Sigma_t \in \mathbb{C}^{M\times M}$ are diagonal matrices with eigenvalues of $\bar{\mathbf{U}}_r$ and $\bar{\mathbf{U}}_t$, respectively. For $\bar{\mathbf{U}}_r$, we utilize the Gaussian randomization to make up a suboptimal solution as $\tilde{\mathbf{u}}_r = \mathbf{V}_r\Sigma_r^{1/2}\kappa_r$, where $\kappa_r \in \mathbb{C}^{(M+1)\times 1}$ is a Gaussian random vector with $\kappa_r \sim \mathcal{CN}(0, \mathbf{I}_{M+1})$. Consequently, the suboptimal reflection matrix can be given by

$$\mathbf{\Phi}_r = \sqrt{\beta_r}\mathrm{diag}\left(e^{j\arg\left(\frac{\tilde{\mathbf{u}}_r[m]}{\tilde{\mathbf{u}}_r[M+1]}\right)}\middle| \forall m \in \mathcal{M}\right), \tag{41}$$

where $\tilde{\mathbf{u}}_r[m]$ is the $m$-th reflecting element of $\tilde{\mathbf{u}}_r$.

For $\bar{\mathbf{U}}_t$, we also utilize the Gaussian randomization to construct a suboptimal solution as $\tilde{\mathbf{u}}_t = \mathbf{V}_t\Sigma_t^{1/2}\kappa_t$ with $\kappa_t \sim \mathcal{CN}(0, \mathbf{I}_M)$. Consequently, the suboptimal transmission matrix can be given by

$$\mathbf{\Phi}_t = \mathrm{diag}\left(e^{j\arg(\tilde{\mathbf{u}}_t)}\right). \tag{42}$$

### D. UAV Location Optimization

For given $\mathbf{\Phi}_r$, $\mathbf{\Phi}_t$, $\mathbf{w}_1$ and $\mathbf{w}_2$, the problem (29) can be reformulated as

$$\max_{\mathbf{q}_a} \ \log_2\left(1+\frac{\left|\left(\mathbf{g}_{rb}^H\mathbf{\Phi}_r\mathbf{g}_{ar}+\mathbf{g}_{ab}^H\right)\mathbf{w}_1\right|^2}{\sigma_b^2}\right) \tag{43a}$$

$$s.t. \ \ \left|\mathbf{g}_{rc}^H\mathbf{\Phi}_t\mathbf{g}_{ar}\mathbf{w}_2\right|^2 \geq \gamma_{thc}\left(\left|\mathbf{g}_{rc}^H\mathbf{\Phi}_t\mathbf{g}_{ar}\mathbf{w}_1\right|^2+\sigma_c^2\right), \tag{43b}$$

$$\left|\left(\mathbf{g}_{rb}^H\mathbf{\Phi}_r\mathbf{g}_{ar}+\mathbf{g}_{ab}^H\right)\mathbf{w}_2\right|^2 \geq \gamma_{thc}\left(\left|\left(\mathbf{g}_{rb}^H\mathbf{\Phi}_r\mathbf{g}_{ar}+\mathbf{g}_{ab}^H\right)\mathbf{w}_1[n]\right|^2+\sigma_b^2\right), \tag{43c}$$

$$\left|\left(\mathbf{g}_{rw}^H\mathbf{\Phi}_r\mathbf{g}_{ar}+\mathbf{g}_{aw}^H\right)\mathbf{w}_1\right|^2 \leq \frac{\left(\rho^{2\epsilon}-1\right)\tilde{\sigma}_w^2}{\rho}. \tag{43d}$$

As $\left|\left(\mathbf{g}_{rb}^H\mathbf{\Phi}_r\mathbf{g}_{ar}+\mathbf{g}_{ab}^H\right)\mathbf{w}_1\right|^2/\sigma_b^2$ increases, the objective function increases, which means that maximizing (43a) is equivalent to maximize $\left|\left(\mathbf{g}_{rb}^H\mathbf{\Phi}_r\mathbf{g}_{ar}+\mathbf{g}_{ab}^H\right)\mathbf{w}_1\right|^2/\sigma_b^2$. However, this form is still difficult to handle. Thus, we introduce an auxiliary variable $t_1$ satisfying $t_1 \leq \left|\left(\mathbf{g}_{rb}^H\mathbf{\Phi}_r\mathbf{g}_{ar}+\mathbf{g}_{ab}^H\right)\mathbf{w}_1\right|^2/\sigma_b^2$. To tackle the non-convexity, we derive it as

$$\left|\left(\mathbf{g}_{rb}^H\mathbf{\Phi}_r\mathbf{g}_{ar}+\mathbf{g}_{ab}^H\right)\mathbf{w}_1\right|^2/\sigma_b^2 = Bd_{ar}^{-2}+2Cd_{ar}^{-1}d_{ab}^{-\nu_1/2}+Dd_{ab}^{-\nu_1}, \tag{44}$$

where the corresponding coefficients can be expressed as

$$B = \rho_0\mathbf{g}_{rb}^H\mathbf{\Phi}_r\mathbf{a}_M^T\mathbf{a}_{N_a}\mathbf{W}_1\mathbf{a}_{N_a}^T\mathbf{a}_M\mathbf{\Phi}_r^H\mathbf{g}_{rb}/\sigma_b^2, \tag{45}$$

$$C = \rho_0\mathcal{R}\left(\mathbf{g}_{rb}^H\mathbf{\Phi}_r\mathbf{a}_M^T\mathbf{a}_{N_a}\mathbf{W}_1\mathbf{h}_{ab}\right)/\sigma_b^2, \tag{46}$$

$$D = \rho_0\mathbf{h}_{ab}^H\mathbf{W}_1\mathbf{h}_{ab}/\sigma_b^2. \tag{47}$$

Therefore, the constraint introduced by the auxiliary variable can be written as

$$t_1 \leq Bd_{ar}^{-2}+2Cd_{ar}^{-1}d_{ab}^{-\nu_1/2}+Dd_{ab}^{-\nu_1} \triangleq \tilde{B}+\tilde{C}+\tilde{D}, \tag{48}$$

where $\tilde{B} = Bd_{ar}^{-2}$, $\tilde{C} = 2Cd_{ar}^{-1}d_{ab}^{-\nu_1/2}$ and $\tilde{D} = Dd_{ab}^{-\nu_1}$. Since the right side of the inequality is not a concave function, (48) is also a non-convex constraint. According to (45) and (47), $B>0$ and $D>0$ hold. Therefore, $\tilde{B}$ and $\tilde{D}$ are convex with respect to $d_{ar}^{-2}$ and $d_{ab}^{-\nu_1}$, respectively. Leveraging the first-order Taylor expansion, the lower bound of $\tilde{B}$ and $\tilde{D}$ can be represented as

$$Bd_{ar}^{-2} \geq B\left(3\bar{d}_{ar}^{-2}-2d_{ar}\bar{d}_{ar}^{-3}\right) \triangleq \bar{B}, \tag{49}$$

$$Dd_{ab}^{-\nu_1} \geq D\left((1+\nu_1)\bar{d}_{ab}^{-\nu_1}-\nu_1 d_{ab}\bar{d}_{ab}^{-\nu_1-1}\right) \triangleq \bar{D}, \tag{50}$$

where $\bar{d}_{ar} = \left\|\mathbf{q}_a^{(r)}-\mathbf{q}_r\right\|$ and $\bar{d}_{ab} = \left\|\mathbf{q}_a^{(r)}-\mathbf{q}_b\right\|$ are the feasible points in the $r$-th iteration. However, it is uncertain that the value of $C$ is positive or negative. In Proposition 1, we transform the non-concave $\tilde{C}$ into a concave form.

**Proposition 1.** *If $C>0$, the non-concave $\tilde{C}$ can be changed*

*into*

$$\begin{aligned}\tilde{C} \geq 2C \Big( & (2+\nu_1/2)\, \bar{d}_{ar}^{-1} \bar{d}_{ab}^{-\nu_1/2} \\ & -\nu_1/2 \bar{d}_{ar}^{-1} \bar{d}_{ab}^{-\nu_1/2-1} d_{ab} - \bar{d}_{ar}^{-2} \bar{d}_{ab}^{-\nu_1/2} d_{ar} \Big) \\ & \triangleq \bar{C}. \end{aligned} \tag{51}$$

*If $C<0$, the non-concave $\tilde{C}$ can be approximated to*

$$\begin{aligned}\tilde{C} & \geq C \left( \left( l_1^{-1} + l_2^{-\nu_1/2} \right)^2 - l_1^{-2} - l_2^{-\nu_1} \right) \\ & \geq C \left( \left( l_1^{-1} + l_2^{-\nu_1/2} \right)^2 - 3\tilde{l}_1^{-2} + 2\tilde{l}_1^{-3} l_1 - (\nu_1+1)\, \tilde{l}_2^{-\nu_1} + \nu_1 \tilde{l}_2^{-\nu_1-1} l_2 \right) \\ & \triangleq \Upsilon, \end{aligned} \tag{52}$$

*where the auxiliary variables $l_1$ and $l_2$ should satisfy*

$$l_1^2 + \|\tilde{\mathbf{q}}_a\|^2 - \|\mathbf{q}_r\|^2 - 2(\tilde{\mathbf{q}}_a - \mathbf{q}_r)^T \mathbf{q}_a \leq 0, \tag{53}$$

$$l_2^2 + \|\tilde{\mathbf{q}}_a\|^2 - \|\mathbf{q}_b\|^2 - 2(\tilde{\mathbf{q}}_a - \mathbf{q}_b)^T \mathbf{q}_a \leq 0. \tag{54}$$

*Proof:* The detailed proof is provided in Appendix D. ■

The non-convex constraint introduced by the auxiliary variable $t_1$ can be transformed into

$$t_1 \leq \bar{B} + \bar{D} + I\bar{C} + (1-I)\, \Upsilon, \tag{55}$$

where $I$ represents a binary variable. When $C>0$, the value of $I$ is 1, and otherwise, $I=0$.

Since $\left|\mathbf{g}_{rc}^H \mathbf{\Phi}_t \mathbf{g}_{ar} \mathbf{w}_1\right|^2 = \rho_0 \left|\mathbf{g}_{rc}^H \mathbf{\Phi}_t \mathbf{a}_M^T \mathbf{a}_{N_a} \mathbf{w}_1\right|^2 d_{ar}^{-2}$ and $\left|\mathbf{g}_{rc}^H \mathbf{\Phi}_t \mathbf{g}_{ar} \mathbf{w}_2\right|^2 = \rho_0 \left|\mathbf{g}_{rc}^H \mathbf{\Phi}_t \mathbf{a}_M^T \mathbf{a}_{N_a} \mathbf{w}_2\right|^2 d_{ar}^{-2}$, the non-convex constraint (43b) can be transformed into

$$\begin{aligned} & \rho_0 \left|\mathbf{g}_{rc}^H \mathbf{\Phi}_t \mathbf{a}_M^T \mathbf{a}_{N_a} \mathbf{w}_2\right|^2 / \sigma_c^2 \\ & \geq \gamma_{thc} \rho_0 \left|\mathbf{g}_{rc}^H \mathbf{\Phi}_t \mathbf{a}_M^T \mathbf{a}_{N_a} \mathbf{w}_1\right|^2 / \sigma_c^2 + \gamma_{thc} d_{ar}^2. \end{aligned} \tag{56}$$

For the non-convex constraint (43c), we have

$$\left|\left(\mathbf{g}_{rb}^H \mathbf{\Phi}_r \mathbf{g}_{ar} + \mathbf{g}_{ab}^H\right) \mathbf{w}_2\right|^2 / \sigma_b^2 = B_3 d_{ar}^{-2} + 2C_3 d_{ar}^{-1} d_{ab}^{-\nu_1/2} + D_3 d_{ab}^{-\nu_1}, \tag{57}$$

where the corresponding coefficients can be given by

$$B_3 = \rho_0 \mathbf{g}_{rb}^H \mathbf{\Phi}_r \mathbf{a}_M^T \mathbf{a}_{N_a} \mathbf{W}_2 \mathbf{a}_{N_a}^T \mathbf{a}_M \mathbf{\Phi}_r^H \mathbf{g}_{rb} / \sigma_b^2, \tag{58}$$

$$C_3 = \rho_0 \mathcal{R}\left(\mathbf{g}_{rb}^H \mathbf{\Phi}_r \mathbf{a}_M^T \mathbf{a}_{N_a} \mathbf{W}_2 \mathbf{h}_{ab}\right) / \sigma_b^2, \tag{59}$$

$$D_3 = \rho_0 \mathbf{h}_{ab}^H \mathbf{W}_2 \mathbf{h}_{ab} / \sigma_b^2. \tag{60}$$

Similarly, since $B_3$ and $D_3$ are positive, we have

$$B_3 d_{ar}^{-2} \geq B_3 \left(3\bar{d}_{ar}^{-2} - 2 d_{ar} \bar{d}_{ar}^{-3}\right) \triangleq \bar{B}_3, \tag{61}$$

$$D_3 d_{ab}^{-\nu_1} \geq D_3 \left((1+\nu_1)\, \bar{d}_{ab}^{-\nu_1} - \nu_1 d_{ab} \bar{d}_{ab}^{-\nu_1-1}\right) \triangleq \bar{D}_3. \tag{62}$$

Then, we analyze the concave form of (59) in Proposition 2.

**Proposition 2.** *If $C_3>0$, we have*

$$\begin{aligned} 2C_3 d_{ar}^{-1} d_{ab}^{-\nu_1/2} \geq & \, 2C_3 \Big( (2+\nu_1/2)\, \bar{d}_{ar}^{-1} \bar{d}_{ab}^{-\nu_1/2} \\ & -\nu_1/2 \bar{d}_{ar}^{-1} \bar{d}_{ab}^{-\nu_1/2-1} d_{ab} - \bar{d}_{ar}^{-2} \bar{d}_{ab}^{-\nu_1/2} d_{ar} \Big) \\ & \triangleq \bar{C}_3. \end{aligned} \tag{63}$$

*If $C_3<0$, we have*

$$\begin{aligned} 2C_3 d_{ar}^{-1} d_{ab}^{-\nu_1/2} \geq & \, C_3 \Big( \left( l_1^{-1} + l_2^{-\nu_1/2} \right)^2 - 3\tilde{l}_1^{-2} + 2\tilde{l}_1^{-3} l_1 \\ & - (\nu_1+1)\, \tilde{l}_2^{-\nu_1} + \nu_1 \tilde{l}_2^{-\nu_1-1} l_2 \Big) \\ & \triangleq \Upsilon_3. \end{aligned} \tag{64}$$

*Proof:* The proof is similar to Proposition 1. ■

Owing to $t_1 \leq \left|\left(\mathbf{g}_{rb}^H \mathbf{\Phi}_r \mathbf{g}_{ar} + \mathbf{g}_{ab}^H\right) \mathbf{w}_1\right|^2 / \sigma_b^2$, the non-convex constraint (43c) can be converted to

$$\bar{B}_3 + \bar{D}_3 + I_3 \bar{C}_3 + (1-I_3)\, \Upsilon_3 \geq \gamma_{thc}\, (t_1+1), \tag{65}$$

where $I_3$ represents a binary variable. When $C_3>0$, the value of $I_3$ is 1. Otherwise, $I_3=0$.

To solve the non-convex constraint (43d), let

$$\left|\left(\mathbf{g}_{rw}^H \mathbf{\Phi}_r \mathbf{g}_{ar} + \mathbf{g}_{aw}^H\right) \mathbf{w}_1\right|^2 = B_2 d_{ar}^{-2} + 2C_2 d_{ar}^{-1} d_{aw}^{-\nu_1/2} + D_2 d_{aw}^{-\nu_1}, \tag{66}$$

where the corresponding coefficients can be represented as

$$B_2 = \rho_0 \mathbf{g}_{rw}^H \mathbf{\Phi}_r \mathbf{a}_M^T \mathbf{a}_{N_a} \mathbf{W}_1 \mathbf{a}_{N_a}^T \mathbf{a}_M \mathbf{\Phi}_r^H \mathbf{g}_{rw}, \tag{67}$$

$$C_2 = \rho_0 \mathcal{R}\left(\mathbf{g}_{rw}^H \mathbf{\Phi}_r \mathbf{a}_M^T \mathbf{a}_{N_a} \mathbf{W}_1 \mathbf{h}_{aw}\right), \tag{68}$$

$$D_2 = \rho_0 \mathbf{h}_{aw}^H \mathbf{W}_1 \mathbf{h}_{aw}. \tag{69}$$

Because $B_2$ and $D_2$ are positive, $B_2 d_{ar}^{-2}$ and $D_2 d_{aw}^{-\nu_1}$ are convex. Nevertheless, we cannot determine whether the value of $C_2$ is positive or negative. When $C_2>0$, $2C_2 d_{ar}^{-1} d_{aw}^{-\nu_1/2} \triangleq \Upsilon_2$ is convex. When $C_2<0$, we have

$$\begin{aligned} 2C_2 d_{ar}^{-1} d_{aw}^{-\nu_1/2} \leq & \, 2C_2 \Big( (2+\nu_1/2)\, \bar{d}_{ar}^{-1} \bar{d}_{aw}^{-\nu_1/2} - \nu_1/2 \bar{d}_{ar}^{-1} \\ & \times \bar{d}_{aw}^{-\nu_1/2-1} d_{aw} - \bar{d}_{ar}^{-2} \bar{d}_{aw}^{-\nu_1/2} d_{ar} \Big) \\ & \triangleq \bar{C}_2, \end{aligned} \tag{70}$$

where $\bar{d}_{aw} = \left\| \mathbf{q}_a^{(r)} - \mathbf{q}_w \right\|$ is the feasible point in the $r$-th iteration and $\bar{C}_2$ is a convex function.

The non-convex constraint (43d) can be transformed into

$$\bar{B}_2 + \bar{D}_2 + I_2 \Upsilon_2 + (1-I_2)\, \bar{C}_2 \leq \frac{\left(\rho^{2\epsilon} - 1\right) \tilde{\sigma}_w^2}{\rho}, \tag{71}$$

where $\bar{B}_2 = B_2 d_{ar}^{-2}$, $\bar{D}_2 = D_2 d_{aw}^{-\nu_1}$, and $I_2$ represents a binary variable. When $C_2>0$, the value of $I_2$ is 1. Otherwise, $I_2=0$.

Consequently, the problem (43) can be reformulated as

$$\max_{\mathbf{q}_a, t_1, l_1, l_2} \; t_1 \tag{72a}$$

$$s.t. \quad (53), (54), (55), (56), (65), (71), \tag{72b}$$

which is a convex problem, and can be tackled by CVX.

### *E. Overall Algorithm*

The original optimization problem is first decoupled into three sub-problems utilizing the BCD. The active and passive beamforming optimization subproblems are solved by the SDR while fixing the other variables. The UAV location optimization subproblem is solved via applying the SCA with the fixed active and passive beamformings. Then, an effective AO algorithm is proposed to iteratively achieve the optimal

solution of the whole problem. The proposed AO algorithm mainly includes five basic steps: initialization, problem decomposition, alternate iteration, updating the solution and convergence check. First, an initial solution is chosen as the starting point of iterations. Then the original optimization problem is decomposed into three subproblems using the BCD algorithm. During the iterations, one optimization subproblem is performed when other variables are fixed. When the optimization of one subproblem is completed, it moves to the next subproblem. The solution of the entire problem is updated and the next iteration continues until the results converge. The proposed AO Algorithm for STAR-RIS aided UAV-NOMA covert communication is described in Algorithm 1.

To analyze the complexity of Algorithm 1, we first consider the complexity of each sub-problem. For the active beamforming optimization subproblem (32), its complexity is $\mathcal{O}_1\left(\sqrt{2N_a+4}\left(n_1\left(2N_a^3+4+n_1\left(2N_a^2+4\right)+n_1^2\right)\right)\right)$, where $\sqrt{2N_a+4}$ denotes the number of iterations, and $n_1 = 2N_a^2$ represents the number of decision variables. Similarly, the complexity of passive beamforming optimization subproblem (38) is $\mathcal{O}_2\left(\sqrt{4M+1}\left(n_2\left(2M^3+3M^2+5M+10+n_2\times\left(2M^2+4M+3\right)+n_2^2\right)\right)\right)$ with $n_2 = 2M^2+2M+3$. The complexity of UAV location optimization subproblem (72) can be expressed as $\mathcal{O}_3\left(\sqrt{6}\left(n_3^3+6n_3^2+6n_3\right)\right)$ with $n_3 = 4$. Consequently, the total complexity for Algorithm 1 is $\mathcal{O}\left(R\left(\mathcal{O}_1+\mathcal{O}_2+\mathcal{O}_3\right)\right)$, where $R$ is the overall iteration number.

**Algorithm 1** AO Algorithm for STAR-RIS aided UAV-NOMA covert communication

1: Initialize $\mathbf{\Phi}_r^0$, $\mathbf{\Phi}_t^0$, $l_1^0$, $l_2^0$, $\mathbf{q}_a^0$. Set the tolerance $\varepsilon_1 = 10^{-4}$ and the number of initial iteration $r = 1$.
2: **repeat**
3: Solve the problem (32) to obtain $\mathbf{W}_1^{(r)}$ and $\mathbf{W}_2^{(r)}$ with given $\mathbf{\Phi}_r^{(r-1)}$, $\mathbf{\Phi}_t^{(r-1)}$ and $\mathbf{q}_a^{(r-1)}$;
4: Obtain $\mathbf{w}_1^{(r)}$ and $\mathbf{w}_2^{(r)}$ by the eigenvalue decomposition;
5: Solve the problem (38) to obtain $\bar{\mathbf{U}}_r^{(r)}$ and $\bar{\mathbf{U}}_t^{(r)}$ with given $\mathbf{w}_1^{(r)}$, $\mathbf{w}_2^{(r)}$ and $\mathbf{q}_a^{(r-1)}$;
6: Obtain $\mathbf{\Phi}_r^{(r)}$ and $\mathbf{\Phi}_t^{(r)}$ by the Gaussian randomization;
7: Solve the problem (72) to obtain $\mathbf{q}_a^{(r)}$ with given $\mathbf{w}_1^{(r)}$, $\mathbf{w}_2^{(r)}$, $\mathbf{\Phi}_r^{(r)}$ and $\mathbf{\Phi}_t^{(r)}$;
8: Calculate the covert transmission rate $R_b^{(r)}$;
9: Update $r = r+1$;
10: **until** The decrease of the objective value is below a threshold $\varepsilon_1$, i.e., $R_b^{(r)} - R_b^{(r-1)} \le \varepsilon_1$.

**Remark 1.** *The convergence analysis is necessary for the proposed AO algorithm. From Algorithm 1, it can be seen that the objective function after each iteration is not lower than the value of the previous iteration, which implies that the objective value is non-decreasing. Because the covert transmission rate has an upper bound, Algorithm 1 is convergent, which will be further verified by simulations.*

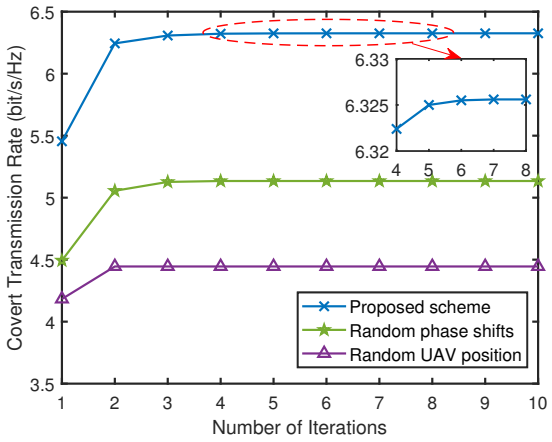


Fig. 2: Convergence of the proposed AO algorithm.

## V. Simulation Results and Discussion

In this section, simulation results are used to prove the effectiveness of the proposed scheme. Unless otherwise stated, the simulation parameters can be found in Table I [34]. In addition, the position of STAR-RIS is $\mathbf{q}_r = [20, 0, 50]^T$m. Bob and Carol are assumed to locate at $\mathbf{q}_b = [30, -10, 0]^T$m and $\mathbf{q}_c = [15, 5, 48]^T$m, respectively. Willie's coordinate is $\mathbf{q}_w = [0, -20, 0]^T$m.

TABLE II: Simulation Parameters

| Parameters | Value |
|---|---|
| Number of antennas | $N_a = 16$ |
| Element number of STAR-RIS | $M = 25$ |
| Noise power | $\sigma_b^2 = \sigma_c^2 = \tilde{\sigma}_w^2 = -90$ dBm |
| Maximum transmit power | $P_a = 10$ dBm |
| Path-loss at the reference distance 1m | $\rho_0 = -30$ dB |
| Path-loss exponent | $\nu_1 = 3$, $\nu_2 = 2.1$ |
| Rician factor | $\mathcal{K} = 3$ |
| Rate threshold of Carol | $R_{thc} = 1$ bit/s/Hz |
| Noise uncertainty level | $\rho = 3$ dB |
| Covertness requirement | $\epsilon = 0.1$ |
| Flight altitude of UAV | $H_a = 80$ m |
| Antenna separation | $\tilde{d} = \lambda/2$ |
| Element spacing of STAR-RIS | $\tilde{d}_x = \tilde{d}_z = \lambda/4$ |

Fig. 2 plots the curve of the covert transmission rate with the number of iterations. We set $P_a = 5$ dBm and $M = 64$. The proposed scheme can converge to a fixed constant after eight iterations, which confirms the previous convergence analysis. In addition, the converging curves of the covert transmission rate with random phase shifts and random UAV position are drawn. These two benchmarks converge a little faster, because the proposed AO algorithm requires three subproblems to work together, which can further enhance the covert transmission rate but reduce the iteration speed.

Fig. 3 depicts the optimal position of UAV after several iterations when the positions of STAR-RIS and users are determined. The initial position of UAV is close to Willie.

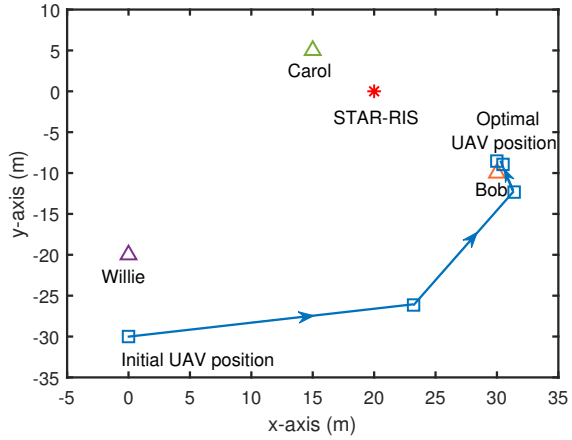


Fig. 3: Optimal UAV position after several iterations.

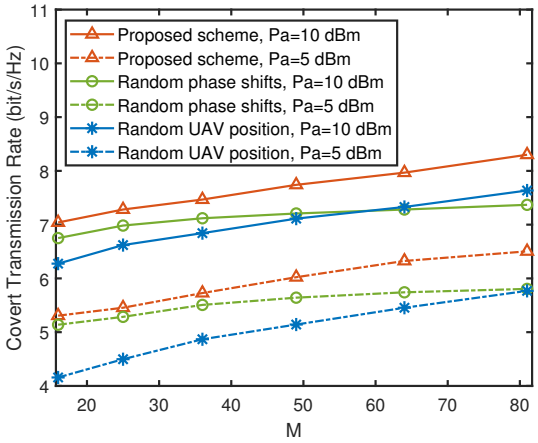


Fig. 5: Covert transmission rate versus the number of STAR-RIS elements with different transmit power.

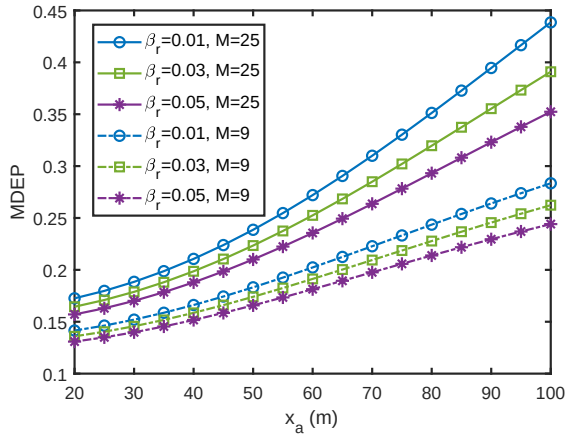


Fig. 4: MDEP versus $x_a$ with different number of STAR-RIS elements and reflected amplitude coefficients.

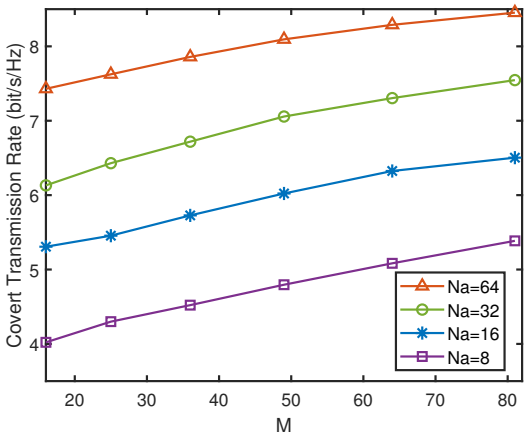


Fig. 6: Covert transmission rate versus the number of STAR-RIS elements with different number of antennas.

Then, UAV moves closer to Bob and away from Willie after each iteration, which makes Willie's detection more difficult while enhancing the covert transmission rate. Finally, UAV hovers between the STAR-RIS and Bob and approaches Bob more closely to maximize the covert transmission rate. At this point, the channel condition at Willie deteriorates; however the double path-loss attenuation caused by STAR-RIS decreases and the channel gain of direct link between UAV and Bob improves, thus increasing the covert transmission rate.

Fig. 4 investigates the effect of UAV position on the MDEP with different number of STAR-RIS elements and reflected amplitude coefficients. The $y$-coordinate of UAV is fixed as $y_a = -20$ m and the transmit power is set to $P_a = 5$ dBm. It can be clearly seen that the MDEP increases as the horizontal coordinate of UAV increases. This is because UAV is moving away from Willie, which indicates that it is more difficult for Willie to detect the covert signal. Therefore, the proper adjustment of UAV position can enhance the covertness. In addition, the MDEP will raise as the number of STAR-RIS elements increases or the reflection coefficient reduces, which suggests that the installation of STAR-RIS is conducive to confusing Willie.

Fig. 5 presents the covert transmission rate versus the number of STAR-RIS elements with different transmit power $P_a = 5$ dBm and $P_a = 10$ dBm. From Fig. 5, it is shown that the covert transmission rate of all schemes can be improved as the number of elements rises. This is because a great deal of elements can bring higher DoF to reconfigure the wireless environment, which enhances the cascaded channel gain. To verify the advantage of the proposed scheme, we also consider two benchmarks: random phase shifts and random UAV position. Compared with the benchmarks, the proposed scheme can provide higher covert transmission rate with different transmit power. It is worth noting that greater transmit power can further enhance the covert transmission rate. As the number of elements increases, the gap between the proposed scheme and random phase shifts becomes larger, because more elements can bring better optimization performance for the passive beamforming.

Fig. 6 investigates the effect of the number of UAV's antennas on the covertness performance with $P_a = 5$ dBm. We can observe that a larger number of antennas will lead to higher covert transmission rate. This is because multiple

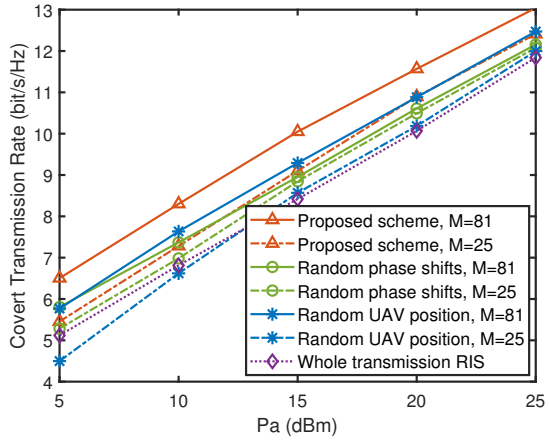


Fig. 7: Covert transmission rate versus the maximum transmit power $P_a$ for different schemes.

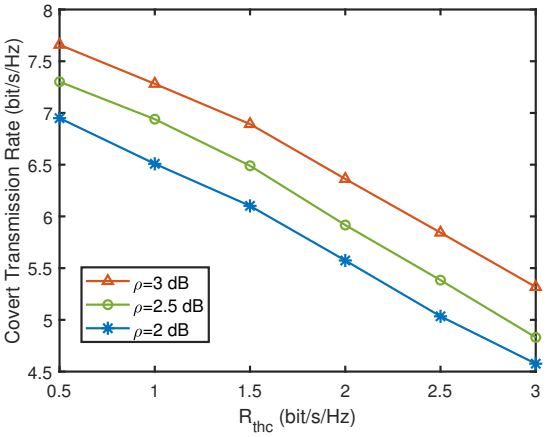


Fig. 8: Covert transmission rate versus the rate threshold of Carol $R_{thc}$ with different noise uncertainty level $\rho$.

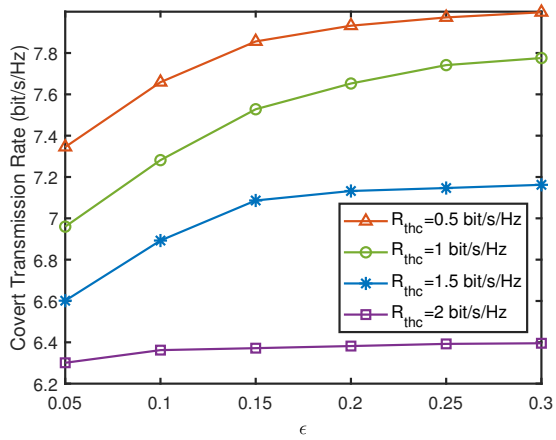


(a)

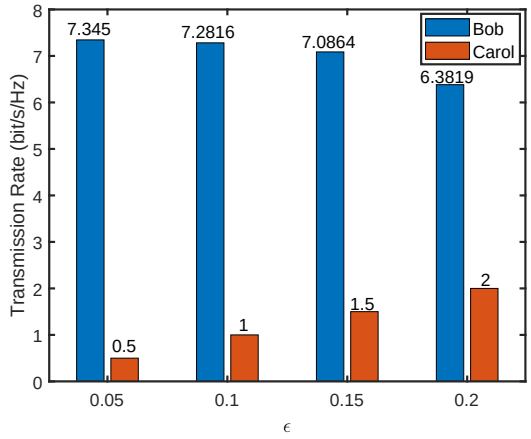


(b)

Fig. 9: (a) Covert transmission rate versus $\epsilon$ with different rate thresholds; (b) Comparison on the transmission rate at Bob and Carol with different covertness requirement $\epsilon$.

antennas can produce additional degree of spatial freedom, which makes the beamforming more precise. More accurate beamforming will contribute to higher receiving SINR, and, the covert transmission rate will be effectively improved.

Fig. 7 compares the covert transmission rate of different schemes as the maximum transmit power $P_a$ grows. The element number of STAR-RIS is set to $M = 25$ and $M = 81$. It can be seen that the covert transmission rate of all schemes can be significantly improved with the transmit power. The covert transmission rate of the proposed scheme is higher than that of the other two random benchmarks. However, the gap of covert transmission rate between $M = 25$ and $M = 81$ in the benchmark of random phase shifts decreases gradually as the transmit power enhances, which is consistent with the curve of the covert transmission rate versus $M$ in Fig. 5. In addition, the covert transmission rate of Bob in UAV-NOMA networks with STAR-RIS is superior compared to those with the whole transmission RIS, which verifies that the STAR-RIS can effectively enhance the covert transmission rate.

Fig. 8 investigates the relationship between the covert transmission rate and the rate threshold of Carol $R_{thc}$ with various noise uncertainty level $\rho$. It can be found from Fig. 8 that the covert transmission rate of Bob decreases obviously with the increase of the rate threshold of Carol. This is due to the fact that as the communication constraint becomes tighter, more power is required for Carol to communicate, and the covert transmission rate at Bob naturally weakens. Furthermore, the covert transmission rate increases with $\rho$ at Willie, since larger noise uncertainty makes the accurate detection of covert transmission more difficult.

Fig. 9(a) illustrates the curve of covert transmission rate for Bob as the covertness requirement $\epsilon$ increases with various rate thresholds for Carol, i.e., $R_{thc} = \{0.5, 1, 1.5, 2\}$ bit/s/Hz. It can be observed from Fig. 9(a) that larger $\epsilon$ can provide higher covert transmission rate. According to the covertness constraint $\xi^* \geq 1 - \epsilon$, a larger $\epsilon$ leads to more relaxed covertness constraint, which can further improve the covert transmission rate. Similarly, as the rate threshold of Carol increases, the communication constraints (29b) and (29c) become tighter, which will give rise to lower covert transmission rate. It is worth noting that when the rate threshold is large, increasing the covertness requirement $\epsilon$ cannot effectively

This article has been accepted for publication in IEEE Journal on Selected Areas in Communications. This is the author's version which has not been fully edited and content may change prior to final publication. Citation information: DOI 10.1109/JSAC.2024.3460079

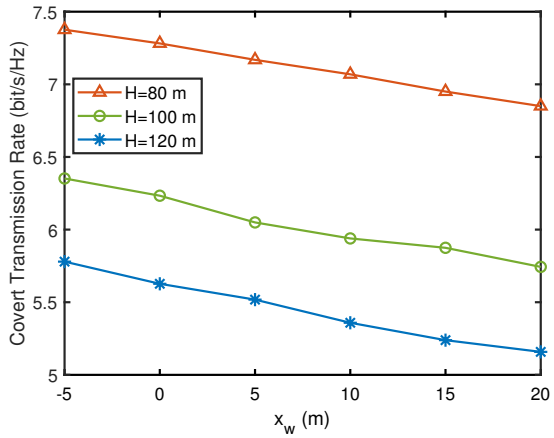


Fig. 10: Covert transmission rate versus $x_w$ with different UAV heights.

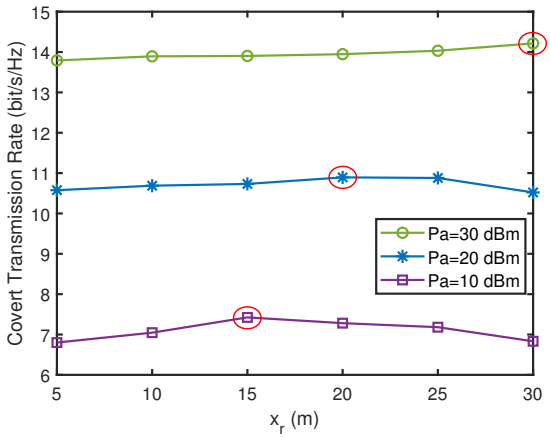


Fig. 11: Covert transmission rate versus $x_r$ with different transmit power.

improve the covert transmission rate of Bob. This is due to that the communication constraints dominate when the rate threshold is large enough, and it is ineffective to relax the covertness constraint to further boost the covert transmission rate. To visualize the rate trade-off between Bob and Carol more intuitively, Fig. 9(b) compares the histograms of the transmission rate at Bob and Carol under different values of the covertness parameter $\epsilon$. Obviously, the transmission rate at Bob and Carol cannot increase at the same time, so there exists a trade-off.

Fig. 10 plots the curve of covert transmission rate as $x$-axis of Willie changes to further explore the effect of Willie's location. The vertical coordinate of Willie is fixed as $y_w = -20$ m. We also compare the effect of UAV with different altitudes on the covert transmission rate. It can be observed that the covert transmission rate decreases as $x$-axis of Willie grows. Based on the topology in Fig. 3, when Willie is getting closer to Bob, the optimal position of UAV cannot be too close to Bob. Therefore, the channel condition of the direct link at Bob deteriorates and the covertness performance is degraded. In addition, higher altitude of UAV leads to lower covert transmission rate. This is mainly because higher altitude brings more path-loss and reduces the channel quality.

Fig. 11 examines the impact of deploying STAR-RIS on the covert transmission rate with different transmit power, i.e., $P_a = \{10, 20, 30\}$ dBm. We fix the $y$-coordinate of STAR-RIS as $y_r = 0$ m and plot the curve of the covert transmission rate versus the horizontal coordinate of STAR-RIS. The results show that the optimal position of STAR-RIS is different with different transmit power. When the transmit power is low, the STAR-RIS should be deployed close to Carol to ensure proper communication with Carol. When the transmit power is large enough, the communication constraint can be satisfied even if it is far away from Carol, which means that deploying the STAR-RIS near Bob will achieve better covert transmission rate. This is because the covertness performance increases as the channel condition at Bob becomes better.

## VI. Conclusion

In this paper, we propose an STAR-RIS aided UAV-NOMA network to realize the covert air-ground transmission. Specifically, Alice sends a public signal to Carol as a cover to achieve the covert transmission between Alice and Bob. Since the closed-form solution of MDEP is difficult to resolve, we utilize the covertness constraint to reduce it to a manageable form. Then, we aim at maximizing the covert transmission rate under the circumstance of ensuring the communication of Carol and meeting the covertness constraint of Bob by jointly optimizing the active and passive beamformings as well as the UAV location. To deal with highly coupled variables, we first apply the BCD to decouple the non-convex problem into three tractable sub-problems. Then, the active and passive beamformings optimization problems are resolved by the SDR, and the UAV location optimization problem is tackled via the SCA. Finally, an effective AO algorithm is presented to iteratively obtain the solution. Simulation results manifest that the proposed scheme can effectively improve the covert transmission rate while guaranteeing the covert transmission between Alice and Bob as well as the public transmission at Carol.

## Appendix A: Proof of Theorem 1

To achieve the optimal detection threshold, we first calculate the DEP $\xi$, which can be given by

$$\xi = 1 - \int_{\max\left(\tau-\phi_1, \frac{1}{\rho}\tilde{\sigma}_w^2\right)}^{\tau-\phi_2} \frac{1}{2\ln(\rho)\, x} dx \tag{A.1}$$

$$= 1 - \frac{1}{2\ln(\rho)} \left( \ln(\tau-\phi_2) - \ln\left( \max\left( \tau-\phi_1, \frac{1}{\rho}\tilde{\sigma}_w^2 \right) \right) \right).$$

Then, the derivative of $\tau$ in (A.1) can be given by

$$\frac{\partial \xi}{\partial \tau} = \begin{cases} -\frac{1}{2\ln(\rho)(\tau-\phi_2)}, & \tau < \phi_1 + \frac{1}{\rho}\tilde{\sigma}_w^2, \\ -\frac{1}{2\ln(\rho)}\left( \frac{1}{(\tau-\phi_2)} - \frac{1}{(\tau-\phi_1)} \right), & \tau \geq \phi_1 + \frac{1}{\rho}\tilde{\sigma}_w^2. \end{cases} \tag{A.2}$$

When $\tau \geq \phi_1 + \frac{1}{\rho}\tilde{\sigma}_w^2$, $\frac{\partial \xi}{\partial \tau} > 0$, and when $\tau < \phi_1 + \frac{1}{\rho}\tilde{\sigma}_w^2$, $\frac{\partial \xi}{\partial \tau} < 0$. This means that $\xi$ first decreases and then increases

with respect to $\tau$. Thus, the DEP is minimum when $\tau = \phi_1 + \frac{1}{\rho}\tilde{\sigma}_w^2$. Owing to $\phi_2 + \frac{1}{\rho}\tilde{\sigma}_w^2 \leq \tau \leq \phi_2 + \rho\tilde{\sigma}_w^2$, the optimal detection threshold can be obtained, which completes the proof of Theorem 1.

## Appendix B: Proof of Theorem 2

Based on (27), it can be observed that $\xi^* = 0$ when $\phi > \tilde{\sigma}_w^2\left(\rho - \frac{1}{\rho}\right)$ holds, which implies Willie can successfully detect the transmission behavior. When $\phi \leq \tilde{\sigma}_w^2\left(\rho - \frac{1}{\rho}\right)$, the MDEP can be given by

$$\xi^* = \int_0^{\tilde{\sigma}_w^2\left(\rho-\frac{1}{\rho}\right)} \left(1 - \frac{1}{2\ln(\rho)} \ln\left(1+\frac{\rho\phi}{\tilde{\sigma}_w^2}\right)\right) f_\phi(\phi)\,\mathrm{d}\phi, \quad \text{(B.1)}$$

where $f_\phi(\phi)$ is PDF of the random variable $\phi$. We define $\phi_0 = \left(\mathbf{g}_{aw}^H + \mathbf{g}_{rw}^H \mathbf{\Phi}_r \mathbf{g}_{ar}\right)\mathbf{w}_1 = \mathbf{g}_{aw}^H \mathbf{w}_1 + \mathbf{g}_{rw}^H \mathbf{\Phi}_r \mathbf{g}_{ar} \mathbf{w}_1$. Based on the large system analytic technique in [35], it is easy to demonstrate that $\phi_0$ follows the complex Gaussian distribution with mean zero and variance $\Delta = \rho_0 d_{aw}^{-v_1} \mathbf{w}_1^H \mathbf{w}_1 + \frac{\rho_0 d_{rw}^{-v_1} \mathbf{w}_1^H \mathbf{w}_1 \mathrm{diag}(\mathbf{\Phi}_r)^H \mathrm{diag}(\mathbf{\Phi}_r)}{M}$. Therefore, the PDF of random variable $\phi = |\phi_0|^2$ can be given by $f_\phi(\phi) = \frac{1}{\Delta} e^{-\frac{\phi}{\Delta}}$. After a series of integral operations, Theorem 2 can be proved.

## Appendix C: Proof of Theorem 3

According to [36], since (32) is a complex-valued homogeneous quadratically constrained quadratic program (QCQP), there exist optimal solutions $\mathbf{W}_1^*$ and $\mathbf{W}_2^*$ satisfying $\mathrm{Rank}^2(\mathbf{W}_1^*) + \mathrm{Rank}^2(\mathbf{W}_2^*) \leq m$, where $m = 4$ in (32) represents the number of constraints after relaxing the rank-one constraint. Furthermore, we aim at maximizing the covert transmission rate under circumstance of meeting users' QoS, which will lead to $\mathbf{W}_1^* \geq 0$ and $\mathbf{W}_2^* \geq 0$. Therefore, $\mathrm{Rank}(\mathbf{W}_1^*) = \mathrm{Rank}(\mathbf{W}_2^*) = 1$ holds. The proof of Theorem 3 is completed.

## Appendix D: Proof of Proposition 1

When $C > 0$, $\tilde{C}$ is convex. (51) can be obtained by the first-order Taylor expansion for $d_{ar}^{-1} d_{ab}^{-\nu_1/2}$. When $C < 0$, we introduce two auxiliary variables $l_1$ and $l_2$ meeting $l_1 \leq d_{ar}$ and $l_2 \leq d_{ab}$. Thus, $l_1^2 \leq d_{ar}^2 = \|\mathbf{q}_a - \mathbf{q}_r\|^2$ and $l_2^2 \leq d_{ac}^2 = \|\mathbf{q}_a - \mathbf{q}_c\|^2$ should be ensured. By the Taylor expansion, we have

$$l_1^2 - \|\tilde{\mathbf{q}}_a - \mathbf{q}_r\|^2 - 2(\tilde{\mathbf{q}}_a - \mathbf{q}_r)^T(\mathbf{q}_a - \tilde{\mathbf{q}}_a) \leq 0, \quad \text{(D.1)}$$

$$l_2^2 - \|\tilde{\mathbf{q}}_a - \mathbf{q}_b\|^2 - 2(\tilde{\mathbf{q}}_a - \mathbf{q}_b)^T(\mathbf{q}_a - \tilde{\mathbf{q}}_a) \leq 0. \quad \text{(D.2)}$$

After simplifying (D.1) and (D.2), (53) and (54) can be proved. Utilizing the auxiliary variables, we can obtain

$$\begin{aligned} 2Cd_{ar}^{-1}d_{ac}^{-\nu_1/2} &\geq 2Cl_1^{-1}l_2^{-\nu_1/2} \\ &\geq C\left(\left(l_1^{-1} + l_2^{-\nu_1/2}\right)^2 - l_1^{-2} - l_2^{-\nu_1}\right) \\ &\overset{(a)}{\geq} C\left(\left(l_1^{-1} + l_2^{-\nu_1/2}\right)^2 - 3\tilde{l}_1^{-2} + 2\tilde{l}_1^{-3}l_1 - (\nu_1+1)\tilde{l}_2^{-\nu_1} + \nu_1\tilde{l}_2^{-\nu_1-1}l_2\right) \\ &\triangleq \Upsilon, \end{aligned} \quad \text{(D.3)}$$

where $(a)$ means the Taylor expansion for $l_1^{-2}$ and $l_2^{-\nu_1}$. To determine the concavity of $\Upsilon$, the Hessian matrix of $\Upsilon$ can be given by (D.4), which shown at the top of the next page. Since $\mathbf{H}(l_1, l_2) < 0$ holds when $C < 0$, $\Upsilon$ is a concave function. Here, the proof of Proposition 1 is finished.

## References


[1] X. You, C.-X. Wang, J. Huang *et al.*, "Towards 6G wireless communication networks: Vision, enabling technologies, and new paradigm shifts," *Sci. China Inf. Sci.*, vol. 64, no. 1, pp. 1–74, Nov. 2020.

[2] M. Mozaffari, W. Saad, M. Bennis, Y.-H. Nam, and M. Debbah, "A tutorial on UAVs for wireless networks: Applications, challenges, and open problems," *IEEE Commun. Surv. Tut.*, vol. 21, no. 3, pp. 2334–2360, thirdquarter 2019.

[3] N. Qi, Z. Huang, F. Zhou, Q. Shi, Q. Wu, and M. Xiao, "A task-driven sequential overlapping coalition formation game for resource allocation in heterogeneous UAV networks," *IEEE Trans. Mobile Comput.*, vol. 22, no. 8, pp. 4439–4455, Aug. 2023.

[4] N. Zhao, W. Lu, M. Sheng, Y. Chen, J. Tang, F. R. Yu, and K.-K. Wong, "UAV-assisted emergency networks in disasters," *IEEE Wireless Commun.*, vol. 26, no. 1, pp. 45–51, Feb. 2019.

[5] Y. Ding, Y. Feng, W. Lu, S. Zheng, N. Zhao, L. Meng, A. Nallanathan, and X. Yang, "Online edge learning offloading and resource management for UAV-assisted MEC secure communications," *IEEE J. Sel. Top. Sign. Proces.*, vol. 17, no. 1, pp. 54–65, Jan. 2023.

[6] H. Lei, H. Yang, K.-H. Park, I. S. Ansari, J. Jiang, and M.-S. Alouini, "Joint trajectory design and user scheduling for secure aerial underlay IoT systems," *IEEE Internet Things J.*, vol. 10, no. 15, pp. 13 637–13 648, Aug. 2023.

[7] R. Li, Z. Wei, L. Yang, D. W. K. Ng, J. Yuan, and J. An, "Resource allocation for secure multi-UAV communication systems with multi-eavesdropper," *IEEE Trans. Commun.*, vol. 68, no. 7, pp. 4490–4506, Jul. 2020.

[8] X. Chen, J. An, Z. Xiong, C. Xing, N. Zhao, F. R. Yu, and A. Nallanathan, "Covert communications: A comprehensive survey," *IEEE Commun. Surveys Tuts.*, vol. 25, no. 2, pp. 1173–1198, 2nd Quart. 2023.

[9] X. Zhou, S. Yan, J. Hu, J. Sun, J. Li, and F. Shu, "Joint optimization of a UAV's trajectory and transmit power for covert communications," *IEEE Trans. Signal Process.*, vol. 67, no. 16, pp. 4276–4290, Aug. 2019.

[10] L. Jiao, R. Zhang, M. Liu, Q. Hua, N. Zhao, A. Nallanathan, and X. Wang, "Placement optimization of UAV relaying for covert communication," *IEEE Trans. Veh. Technol.*, vol. 71, no. 11, pp. 12 327–12 332, Nov. 2022.

[11] M. Li, X. Tao, H. Wu, and N. Li, "Joint trajectory and resource optimization for covert communication in UAV-enabled relaying systems," *IEEE Trans. Veh. Technol.*, vol. 72, no. 4, pp. 5518–5523, Apr. 2023.

[12] G. Yang, Y. Qian, K. Ren, Z. Mei, F. Shu, X. Zhou, and W. Wu, "Covert wireless communications for augmented reality systems with dual cooperative UAVs," *IEEE J. Sel. Top. Sign. Proces.*, vol. 17, no. 5, pp. 1119–1130, Sept. 2023.

[13] J. Hu, M. Guo, S. Yan, Y. Chen, X. Zhou, and Z. Chen, "Deep reinforcement learning enabled covert transmission with UAV," *IEEE Wireless Commun. Lett.*, vol. 12, no. 5, pp. 917–921, May 2023.

[14] P. S. Bithas, V. Nikolaidis, A. G. Kanatas, and G. K. Karagiannidis, "UAV-to-ground communications: Channel modeling and UAV selection," *IEEE Trans. Commun.*, vol. 68, no. 8, pp. 5135–5144, Aug. 2020.

[15] Q. Wu and R. Zhang, "Towards smart and reconfigurable environment: Intelligent reflecting surface aided wireless network," *IEEE Commun. Mag.*, vol. 58, no. 1, pp. 106–112, Jan. 2020.

[16] M. Wu, Y. Xiao, Y. Gao, and M. Xiao, "Digital twin for UAV-RIS assisted vehicular communication systems," *IEEE Trans. Wireless Commun.*, vol. 23, no. 7, pp. 7638–7651, Jul. 2024.

[17] Z. Chen, G. Chen, J. Tang, S. Zhang, D. K. So, O. A. Dobre, K.-K. Wong, and J. Chambers, "Reconfigurable-intelligent-surface-assisted B5G/6G wireless communications: Challenges, solution, and future opportunities," *IEEE Commun. Mag.*, vol. 61, no. 1, pp. 16–22, Jan. 2023.

[18] M. Wu, Y. Xiao, Y. Gao, and M. Xiao, "Design of reconfigurable intelligent surface-aided cross-media communications," *IEEE Trans. Commun.*, vol. 70, no. 12, pp. 8433–8447, Dec. 2022.

[19] C. Huang, R. Mo, and C. Yuen, "Reconfigurable intelligent surface assisted multiuser MISO systems exploiting deep reinforcement learning," *IEEE J. Sel. Areas Commun.*, vol. 38, no. 8, pp. 1839–1850, Aug. 2020.

$$\mathbf{H}\left(l_1, l_2\right) = \begin{bmatrix} C\left(6l_1^{-4} + 4l_2^{-\nu_1/2} l_1^{-3}\right) & Cvl_2^{-\nu_1/2-1} l_1^{-2} \\ Cvl_2^{-\nu_1/2-1} l_1^{-2} & C\left(\left(\nu_1^2/2 + v\right) l_1^{-1} l_2^{-\nu_1/2-2} + \left(\nu_1^2 + \nu_1\right) l_2^{-\nu_1-2}\right) \end{bmatrix}. \tag{D.4}$$


[20] Y. Liu, X. Mu, J. Xu, R. Schober, Y. Hao, H. V. Poor, and L. Hanzo, "STAR: Simultaneous transmission and reflection for 360° coverage by intelligent surfaces," *IEEE Wireless Commun.*, vol. 28, no. 6, pp. 102–109, Dec. 2021.

[21] W. Du, Z. Chu, G. Chen, P. Xiao, Y. Xiao, X. Wu, and W. Hao, "STAR-RIS assisted wireless powered IoT networks," *IEEE Trans. Veh. Technol.*, vol. 72, no. 8, pp. 10 644–10 658, Aug. 2023.

[22] Q. Wang, X. Pang, C. Wu, L. Xu, N. Zhao, and F. R. Yu, "Transmit power minimization for STAR-RIS aided FD-NOMA networks," *IEEE Trans. Veh. Technol.*, vol. 73, no. 3, pp. 4389–4394, Mar. 2024.

[23] J. Lei, T. Zhang, X. Mu, and Y. Liu, "NOMA for STAR-RIS assisted UAV networks," *IEEE Trans. Commun.*, vol. 72, no. 3, pp. 1732–1745, 2024.

[24] Y. Su, X. Pang, W. Lu, N. Zhao, X. Wang, and A. Nallanathan, "Joint location and beamforming optimization for STAR-RIS aided NOMA-UAV networks," *IEEE Trans. Veh. Technol.*, vol. 72, no. 8, pp. 11 023–11 028, Aug. 2023.

[25] P. Zhu, L. Qin, J. Wang, Y. Li, X. Li, and W. Xie, "Optimized trajectory and passive beamforming for STAR-RIS-assisted UAV-empowered O2I WPCN," *IEEE Wireless Commun. Lett.*, vol. 13, no. 1, pp. 163–167, Jan. 2024.

[26] H. Xiao, X. Hu, P. Mu, W. Zhang, W. Wang, K.-K. Wong, and K. Yang, "STAR-RIS enhanced UAV-enabled MEC networks with bi-directional task offloading," [Online] Available: https://arxiv.org/abs/2401.05725.

[27] X. Wang, Z. Lin, F. Lin, and P. Xiao, "Quantum sensing based joint 3D beam training for UAV-mounted STAR-RIS aided Tera-Hertz multi-user massive MIMO systems," [Online] Available: https://arxiv.org/abs/2212.07731.

[28] W. Wang, W. Ni, H. Tian, and L. Song, "Intelligent omni-surface enhanced aerial secure offloading," *IEEE Trans. Veh. Technol.*, vol. 71, no. 5, pp. 5007–5022, May 2022.

[29] A. M. Benaya, M. H. Ismail, A. S. Ibrahim, and A. A. Salem, "Physical layer security enhancement via intelligent omni-surfaces and UAV-friendly jamming," *IEEE Access*, vol. 11, pp. 2531–2544, 2023.

[30] L. Guo, J. Jia, J. Chen, and X. Wang, "Secure communication optimization in NOMA systems with UAV-mounted STAR-RIS," *IEEE Trans. Inf. Forensics Security*, vol. 19, pp. 2300–2314, 2024.

[31] L. Lv, Q. Wu, Z. Li, Z. Ding, N. Al-Dhahir, and J. Chen, "Covert communication in intelligent reflecting surface-assisted NOMA systems: Design, analysis, and optimization," *IEEE Trans. Wireless Commun.*, vol. 21, no. 3, pp. 1735–1750, Mar. 2022.

[32] J. Si, Z. Li, Y. Zhao, J. Cheng, L. Guan, J. Shi, and N. Al-Dhahir, "Covert transmission assisted by intelligent reflecting surface," *IEEE Trans. Commun.*, vol. 69, no. 8, pp. 5394–5408, Aug. 2021.

[33] T.-X. Zheng, H.-M. Wang, D. W. K. Ng, and J. Yuan, "Multi-antenna covert communications in random wireless networks," *IEEE Trans. Wireless Commun.*, vol. 18, no. 3, pp. 1974–1987, Mar. 2019.

[34] J. Si, Z. Li, Y. Zhao, J. Cheng, L. Guan, J. Shi, and N. Al-Dhahir, "Covert transmission assisted by intelligent reflecting surface," *IEEE Trans. Commun.*, vol. 69, no. 8, pp. 5394–5408, Aug. 2021.

[35] H. Xiao, X. Hu, P. Mu, W. Wang, T.-X. Zheng, K.-K. Wong, and K. Yang, "Simultaneously transmitting and reflecting RIS (STAR-RIS) assisted multi-antenna covert communication: Analysis and optimization," *IEEE Trans. Wireless Commun.*, vol. 23, no. 6, pp. 6438–6452, Jun. 2024.

[36] Z.-Q. Luo, W.-K. Ma, A. M.-C. So, Y. Ye, and S. Zhang, "Semidefinite relaxation of quadratic optimization problems," *IEEE Signal Process. Mag.*, vol. 27, no. 3, pp. 20–34, May 2010.


**Qunshu Wang** received the M.S. degree from Henan Polytechnic University in 2022. She is currently pursuing the Ph.D. degree with the School of Information and Communication Engineering, Dalian University of Technology, China. Her current research interests include unmanned aerial vehicle communications, covert communication and simultaneously transmitting and reflecting reconfigurable intelligent surface.

**Shaoyong Guo** (Member, IEEE) is a professor at the School of Computer Science, Beijing University of Posts and Telecommunications. He received the National Science Fund for Excellent Young Scholars in 2023. His research interests include DPU, Blockchain Application technology, Edge Intelligence, and so on. He has achieved innovative results such as power communication network convergence control model and method, network data trusted sandbox privacy sharing service mechanism and technology, and edge security protection technology and mechanism in an open network environment. He is undertaking many key research and development projects and fund projects, and contributed to a number of pioneering standards proposals in ITU-T. The systems and devices developed by him have large-scale application. He was awarded the second prize of Science and Technology Progress Award of Beijing Municipality, Henan Province and Jiangsu Province, and the second prize of Science and Technology Progress Award of Chinese Institute of Electronics, and so on.

**Celimuge Wu** (Senior Member, IEEE) received his PhD degree from The University of Electro-Communications, Japan. He is currently a professor and the director of Meta-Networking Research Center, The University of Electro-Communications. His research interests include Vehicular Networks, Edge Computing, IoT, and AI for Wireless Networking and Computing. He serves as an associate editor of IEEE Transactions on Cognitive Communications and Networking, IEEE Transactions on Network Science and Engineering, and IEEE Transactions on Green Communications and Networking. He is Vice Chair (Asia Pacific) of IEEE Technical Committee on Big Data (TCBD). He is a recipient of 2021 IEEE Communications Society Outstanding Paper Award, 2021 IEEE Internet of Things Journal Best Paper Award, IEEE Computer Society 2020 Best Paper Award and IEEE Computer Society 2019 Best Paper Award Runner-Up. He is an IEEE Vehicular Technology Society Distinguished Lecturer.

**Chengwen Xing** (Member, IEEE) received the B.Eng. degree from Xidian University, Xi'an, China, in 2005, and the Ph.D. degree from the University of Hong Kong, Hong Kong, China, in 2010. Since September 2010, he has been with the School of Information and Electronics, Beijing Institute of Technology, Beijing, China, where he is currently a Full Professor. His current research interests include machine learning, statistical signal processing, convex optimization, multivariate statistics, and array signal processing.

**Nan Zhao** (Senior Member, IEEE) is currently a Professor at Dalian University of Technology, China. He received the Ph.D. degree in information and communication engineering in 2011, from Harbin Institute of Technology, Harbin, China. Dr. Zhao is serving on the editorial boards of IEEE Wireless Communications and IEEE Wireless Communications Letters. He won the best paper awards in IEEE VTC 2017 Spring, ICNC 2018, WCSP 2018 and WCSP 2019. He also received the IEEE Communications Society Asia Pacific Board Outstanding Young Researcher Award in 2018.

**Dusit Niyato** (Fellow, IEEE) is a professor in the College of Computing and Data Science, at Nanyang Technological University, Singapore. He received B.Eng. from King Mongkuts Institute of Technology Ladkrabang (KMITL), Thailand and Ph.D. in Electrical and Computer Engineering from the University of Manitoba, Canada. His research interests are in the areas of mobile generative AI, edge intelligence, decentralized machine learning, and incentive mechanism design.

**George K. Karagiannidis** (Fellow, IEEE) is currently Professor in the Electrical and Computer Engineering Dept. of Aristotle University of Thessaloniki, Greece and Head of Wireless Communications & Information Processing (WCIP) Group. He is also Faculty Fellow in the Artificial Intelligence & Cyber Systems Research Center, Lebanese American University. His research interests are in the areas of Wireless Communications Systems and Networks, Signal processing, Optical Wireless Communications, Wireless Power Transfer and Applications and Communications & Signal Processing for Biomedical Engineering. Dr. Karagiannidis is the Editor-in Chief of IEEE Transactions on Communications and in the past was the Editor-in Chief of IEEE Communications Letters. Recently, he received three prestigious awards: The 2021 IEEE ComSoc RCC Technical Recognition Award, the 2018 IEEE ComSoc SPCE Technical Recognition Award and the 2022 Humboldt Research Award from Alexander von Humboldt Foundation. Dr. Karagiannidis is one of the highly-cited authors across all areas of Electrical Engineering, recognized from Clarivate Analytics as Web-of-Science Highly-Cited Researcher in the nine consecutive years 2015-2023.